Accepted Manuscript

Lasing the DNA fragments through β-diketimine framed Knoevenagel condensed Cu(II) and Zn(II) complexes – An *in vitro* and *in vivo* approach

Natarajan Raman, Narayanaperumal Pravin

PII: S1386-1425(13)01116-5
DOI: http://dx.doi.org/10.1016/j.saa.2013.09.109
Reference: SAA 11088

To appear in: *Spectrochimica Acta Part A: Molecular and Biomolecular Spectroscopy*

Received Date: 23 July 2013
Revised Date: 10 September 2013
Accepted Date: 26 September 2013

Please cite this article as: N. Raman, N. Pravin, Lasing the DNA fragments through β-diketimine framed Knoevenagel condensed Cu(II) and Zn(II) complexes – An *in vitro* and *in vivo* approach, *Spectrochimica Acta Part A: Molecular and Biomolecular Spectroscopy* (2013), doi: http://dx.doi.org/10.1016/j.saa.2013.09.109

Lasing the DNA fragments through β-diketimine framed Knoevenagel condensed Cu(II) and Zn(II) complexes – An *in vitro* and *in vivo* approach

Natarajan Raman,* Narayanaperumal Pravin

Research Department of Chemistry, VHNSN College, Virudhunagar-626 001, Tamil Nadu, India,

E-mail: ramchem1964@gmail.com Tel: +091-92451-65958
E-mail: pravinknp2012@gmail.com Tel: +091-9677846333

ABSTRACT

The syntheses, structures and spectroscopic properties of Cu(II) and Zn(II) complexes having Knoevenagel condensate β-diketimine Schiff base ligands have been investigated in this paper. Characterization of these complexes was carried out using FTIR, NMR, UV–Vis., elemental analysis, mass and EPR techniques. Absorption titration, electrochemical analyses and viscosity measurements have also been carried out to determine the mode of binding. The shift in ΔEp, $E_{1/2}$ and Ip_c values explores the interaction of CT DNA with the above metal complexes. Interaction of ligands and their complexes with DNA revealed an intercalative mode of binding between them. Antimicrobial studies showed an effective antimicrobial activity of the metal ions after coordination with the ligands. The antioxidant properties of the Schiff base ligands and their complexes were evaluated in a series of *in vitro* tests by using 1,1-diphenyl-2-picrylhydrazyl ($DPPH^{\bullet}$) and H_2O_2 free radical scavengers. *In vivo* and *in vitro* antitumor functions of the complexes against Ehrlich ascites carcinoma tumor model have also been investigated. All the results support that β–diketone derived Knoevenagel condensate Schiff base complexes may act as novel antitumor drugs and suggest that their potent cell life inhibition may contribute to their anti-cancer efficacy.

Keywords:
β-diketimine; intercalative mode; antimicrobial studies; antioxidant properties; antitumor activity

**Corresponding author: E-mail: ramchem1964@gmail.com (N.Raman)*
Tel.: +091-092451-65958; Fax: +091-4562-281338

1. Introduction

Medicinal researchers are continuing all over world in order to explore a safe and effective metal based biologically active compound as potential antitumor drug which is of great urgency to overcome the drug-induced cellular resistance and the efficacy of each drug against certain cancers. The treatment involves the administration of multiple drugs as it is clear that chemotherapy leads to the development of resistance. As the first generation of the platinum-based antitumor agent, cisplatin is widely used in the treatment of head and neck, testicular, small lung cell and ovarian cancers [1–4]. In spite of its success, the clinical application of cisplatin is greatly restricted by its toxicity, low water-solubility, instinct and acquired drug resistance [5,6]. Thousands of platinum compounds have been synthesized and screened for their antitumor activity, but little success has been achieved so far in finding novel platinum-based drugs active towards cisplatin resistant/refractory tumors [7,8]. Non-platinum active compounds are likely to have mechanism of action, bio distribution and toxicity which are different from those of platinum drugs and might be effective against human cancers that are poor chemosensitive or have become resistant to conventional platinum drugs. Among the different therapeutic strategies to eradicate cancer cells through DNA damage, the view of using transition metal complexes, capable of oxidative or hydrolytic DNA cleavage as anti-cancer drugs, is a challenging topic in bioinorganic chemistry [9, 10]. Recently, there has been tremendous interest in studies related to the interaction of transition metal ions with nucleic acid because of their relevance in the development of new reagents for biotechnology and medicine [11]. These studies are also important to understand the toxicity of drugs containing metal ions [12]. β-Diketimines are versatile ligand systems which have been known to form complexes with almost every metal ion and metalloid [13]. Earlier reports indicate that the attempts to prepare highly symmetrical and conjugated macrocyclic systems derived from β-diketones condensed with organic amines have not led to the desired results. Condensation of the active methylene group of the β-diketone with an aldehydic group gives a non-enolisable Knoevenagel condensate, which can effectively react with amines to form Schiff bases [14]. Metal complexes of β-diketone derivatives have played an important role in coordination chemistry [15–17] and have been widely used in various aspects of industries, such as organic electroluminescent technology, luminescent materials and sensors for bioinorganic applications [18–20]. With an

aim to develop cis-platin type anti-tumor response of β-diketone, different aromatic aldehydes are introduced in active methylene group by Knoevenagel condensation. β-Diketone derived complexes show antimicrobial, anti-malarial and antitumorous activities, antioxidant, insecticidal activity. Recently transition metal complexes have received considerable interest in nucleic acid chemistry because of their chelating nature. The coordination behavior of β-diketimine also has significant influences in the relative stabilities of the Schiff base complexes as well as their use in biomedicine [21–24]. Thus, scientists are now engaged to explore the transition metal based complexes. Hence, the higher degree of conjugated versatile ligand systems of the Knoevenagel condensate β-diketimine as Schiff bases containing electron releasing/electron withdrawing groups and their low molecular weight copper(II) and zinc(II) complexes have been synthesized. It is therefore of interest to carryout investigations on model compounds to understand how a ligand environment could affect the redox properties of the central metal and thereby, the spectral properties and also interested to explore the DNA binding and DNA cleavage activity of synthesized complexes. This result would be helpful for understanding the binding mode of the complexes to DNA and it also lays a foundation for developing new useful DNA probes and effective inorganic complex nucleases.

2. Experimental protocols

2.1. Reagents and instruments

All reagents, benzaldehyde, acetylacetone, *para* substituted anilines and metal(II) chlorides were of Merck products and they were used as supplied. Commercial solvents were distilled and then used for the preparation of ligands and their complexes. DNA was purchased from Bangalore Genei (India). Microanalyses (C, H and N) were performed in Carlo Erba 1108 analyzer at Sophisticated Analytical Instrument Facility (SAIF), Central Drug Research Institute (CDRI), Lucknow, India. Molar conductivities in DMF (10^{-3} M) at room temperature were measured by using Systronic model-304 digital conductivity meter. Magnetic susceptibility measurement of the complexes was carried out by Gouy balance using copper sulphate pentahydrate as the calibrant. Infrared spectra (4000–350 cm^{-1} KBr disc) of the samples were recorded on an IR Affinity-1 FT-IR Shimadzu spectrophotometer. NMR spectra were recorded on a Bruker Avance Dry 300 FT-NMR spectrometer in DMSO-d_6, using TMS as the internal reference. Mass spectrometry experiments were performed on a JEOL-AccuTOF JMS-T100LC

mass spectrometer equipped with a custom-made electrospray interface (ESI). EPR spectra were recorded on a Varian E 112 EPR spectrometer in DMSO solution both at room temperature (300 K) and liquid nitrogen temperature (77 K) using TCNE (tetracyanoethylene) as the g-marker. The absorption spectra were recorded by using Shimadzu model UV-1601 spectrophotometer at room temperature.

2.2. Synthesis of 3-benzylidenepentane-2,4-dione

The non-enolisable β-diketone was prepared by employing the modified procedure reported earlier [25]. Pentane-2,4-dione (10 mmol) was mixed with benzaldehyde (10 mmol) and piperidine (0.2 mL), and the reaction mixture was stirred thoroughly for *ca.* 5 h with occasional cooling. Yellow colored crystalline solid was obtained after two weeks on keeping in the refrigerator which was filtered, washed with ethanol followed by an excess of petroleum-ether to remove any unreacted reagent. Washing was repeated for two or three times and then the compound was recrystallized from ethylacetate–petroleum ether mixture to get a pure yellow solid, Knoevenagel condensate [*3-benzylidenepentane-2,4-dione*]. It was used as the starting material for the preparation of Schiff base.

Yield: 73%. Anal. Calc. for $C_{12}H_{12}O_2$: C, 76.6; H, 6.5; Found: C, 75.8; H, 6.1 (%). IR (KBr pellet, cm^{-1}): 1718 ν(–C=O), 1494 ν(–HC=C). ^{1}H–NMR (δ): (aromatic, 6H) 7.0–7.4 (m); (–C=CH–, 1H), 8.3 (s); (–CH_3), 2.3 (s). ^{13}C–NMR (δ): 126.0–128.0 (C_1 to C_3), 134.7 (C_4), 129.0 (C_5), 140.6 (C_6), 143.7 (C_7), 198.6 (C_8), 28.3. MS m/z (%): 189 $[M+1]^+$.

2.3. Synthesis of Schiff bases

The Schiff base was prepared by dissolving *3-benzylidenepentane-2,4-dione* (10 mmol) in ethanol and refluxed with *p*-substituted (X) aniline where X = –NO_2 (L^1), –H (L^2), –OH (L^3) and –OCH_3 (L^4) (20 mmol) in ethanol after the addition 0.5 g of anhydrous K_2CO_3 for *ca.* 6 h. The K_2CO_3 was filtered off from the reaction mixture. The dark brown solution was set aside to evaporate and the dark brown solid that separated was filtered off and recrystallized from ethanol and dried in *vacuo*.

L^1. Yield: 68%. Anal. Calc. for $C_{24}H_{20}N_4O_4$: C, 67.3; H, 4.7; N, 13.1 (%); Found: C, 66.5; H, 4.5; N, 12.4 (%). IR (KBr pellet, cm^{-1}): 1631 ν(–C=N); 1502 ν(–HC=C);1473, 1307,840 ν(–C–N ring str; –NO_2).^{1}H–NMR (δ): (aromatic) 6.9–7.3 (m); (–CH_3, 6H), 2.1 (s). ^{13}C–NMR (δ): 125.0–

127.0 (C_1 to C_3), 134.1 (C_4), 136.6 (C_5), 114.3 (C_6), 175.4 (C_7), 20.4 (C_8), 153.4 (C_9), 123.2 (C_{10}), 125.1 (C_{11}) 146.4 (C_{12}). MS m/z (%): 429 $[M+1]^+$. λ_{max} (cm^{-1}) in EtOH, 45857, 27132.

L^2. Yield: 66%. Anal. Calc. for $C_{24}H_{22}N_2$: C, 85.2; H, 6.6; N, 8.3; Found: C, 85.1; H, 6.5; N, 8.1 IR (KBr pellet, cm^{-1}): 1509 ν(–HC=C–); 1632 ν(–C=N). ^{1}H–NMR (δ, ppm): (aromatic) 6.9–7.2 (m); (–CH_3, 6H), 2.3 (s). ^{13}C–NMR (δ, ppm):125.0–129.0 (C_1 to C_3), 133.4 (C_4), 136.2 (C_5), 112.4 (C_6), 173.9 (C_7), 20.3 (C_8), 137.1 (C_9), 119.6 (C_{10}), 131.4 (C_{11}), 128.7 (C_{12}). MS m/z (%): 339 $[M+1]^+$. λ_{max} (cm^{-1}) in EtOH, 42783, 28324.

L^3. Yield: 63%. Anal. Calc. for $C_{24}H_{22}N_2O_2$: C, 77.8; H, 5.9; N, 7.6; Found: C, 77.3; H, 5.8; N, 7.4 (%). IR (KBr pellet, cm^{-1}): 3430 ν(–OH); 1638 ν(–C=N); 1525 ν(–HC=C). ^{1}H–NMR (δ, ppm): (aromatic) 6.9-7.4 (m); (–OH, 1H) 10.3 (s); (–CH_3, 6H), 2.2 (s). ^{13}C–NMR (δ, ppm): 125.2–128.0 (C_1 to C_3), 134.3 (C_4), 136.2 (C_5), 114.1 (C_6), 175.2 (C_7), 20.2 (C_8), 147.6 (C_9), 122.9 (C_{10}), 118.4 (C_{11}), 154.8 (C_{12}). MS m/z (%): 371 $[M+1]^+$. λ_{max} (cm^{-1}) in EtOH, 44768, 28237.

L^4. Yield: 64%. Anal. Calc. for $C_{26}H_{26}N_2O_2$: C, 78.4; H, 6.6; N, 7.0; Found: C, 78.2; H, 6.4; N, 6.7 (%). IR (KBr pellet, cm^{-1}): 1635 ν(–C=N); 1541 ν(–HC=C); 1273, 1083 ν(–C–O–C–). ^{1}H–NMR (δ): (aromatic) 6.9–7.3 (m); (–CH_3, 6H), 2.4 (s); 3.8 (–OCH_3, 6H). ^{13}C–NMR (δ):125.0–129.0 (C_1 to C_3), 132.9 (C_4), 137.2 (C_5), 112.7 (C_6), 172.8 (C_7), 20.6 (C_8), 142.4 (C_9), 122.1 (C_{10}), 116.5 (C_{11}), 158.6 (C_{12}), 58.3 (C_{13}). MS m/z (%): 399 $[M+1]^+$. λ_{max} (cm^{-1}) in EtOH, 41656, 28014.

2.4. Synthesis of metal complexes

To a stirred ethanolic solution of the above Schiff base(s) (5 mmol), a solution of copper(II)/zinc(II) chloride (5 mmol) in ethanol was added dropwise. The reaction solution was refluxed for 2 h. After cooling the reaction mixture to an ambient temperature, the formed solid was filtered, washed with diethyl ether and finally dried *in vacuum*.

[CuL^1Cl_2]. Yield: 65%. Anal. Calc. for $C_{24}H_{20}N_4O_4CuCl_2$: Cu, 11.3; C, 51.2; H, 3.6; N, 9.9; Found: Cu, 11.2; C, 51.1; H, 3.6; N, 9.8 (%). IR (KBr pellet, cm^{-1}): 1603 ν(–C=N); 1497 ν(–HC=C); 1472, 1306, 843 ν(–C–N str; –NO_2); 423 (M–N). MS m/z (%): 562 $[M+1]^+$. Λ_M 10^{-3}(ohm^{-1} cm^2 mol^{-1}) = 5.5. λ_{max} in DMF, 43928, 35116, 17457. μ_{eff} (BM): 1.84.

[CuL^2Cl_2]. Yield: 62%.). Anal. Calc. for $C_{24}H_{22}N_2CuCl_2$: Cu, 13.4; C, 61.0; H, 4.7; N, 5.9; Found: Cu, 13.4; C, 60.9; H, 4.6; N, 5.8 (%). IR (KBr pellet, cm^{-1}): 1608 ν(C=N); 1507

ν(–HC=C); 437 (M–N). MS m/z (%): 472 $[M+1]^+$. Λ_M 10^{-3} (ohm^{-1} cm^2 mol^{-1}) = 9.2 λ_{max} (cm^{-1}) in DMF, 40263, 29359, 18264. μ_{eff} (BM): 1.87.

[CuL^3Cl_2]. Yield: 59%.). Anal. Calc. for $C_{24}H_{22}N_2O_2CuCl_2$: Cu, 12.6; C, 57.1; H, 4.4; N, 5.6; Found: Cu, 12.5; C, 56.9; H, 4.4; N, 5.5 (%). IR (KBr pellet, cm^{-1}): 1612 ν(–C=N); 1522 ν(–HC=C); 3430 ν(–OH); 441 (M–N). MS m/z (%): 504 $[M+1]^+$. Λ_M 10^{-3} (ohm^{-1} cm^2 mol^{-1}) = 4.3. λ_{max} (cm^{-1}) in DMF, 41543, 33245, 17176. μ_{eff} (BM): 1.83.

[CuL^4Cl_2]. Yield: 51%. Anal. Calc. for $C_{26}H_{26}N_2O_2CuCl_2$: Cu, 11.9; C, 59.0; H, 4.9; N, 5.3; Found: Cu, 11.8; C, 58.5; H, 4.9; N, 5.2 (%). IR (KBr pellet, cm^{-1}): 1609 ν(–C=N); 1538 ν(–HC=C); 1269, 1081,ν(–C–O–C–); 428 (M–N). MS m/z (%): 532 $[M+1]^+$. Λ_M 10^{-3} (ohm^{-1} cm^2 mol^{-1}) = 3.9. λ_{max} (cm^{-1}) in DMF, 41727, 31429, 18426. μ_{eff} (BM): 1.81

[ZnL^1Cl_2]. Yield: 63%. Anal. Calc. for $C_{24}H_{20}N_4O_4ZnCl_2$: Zn, 11.6; C, 51.0; H, 3.6; N, 10.0; Found: Zn, 11.5; C, 50.9; H, 3.5; N, 9.9 (%). IR (KBr pellet, cm^{-1}): 1610 ν(–C=N); 1501 ν(–HC=C); 1469, 1309, 838 ν(–C–N str; $–NO_2$); 427 (M–N). ^{1}H–NMR (δ): (aromatic) 6.9–7.2 (m); ($–CH_3$, 6H), 2.0 (s). ^{13}C–NMR (δ): 124.9–126.2 (C_1 to C_3), 134.1 (C_4), 136.4 (C_5), 114.1 (C_6), 169.2 (C_7), 20.1 (C_8), 153.2 (C_9), 123.1 (C_{10}), 124.9 (C_{11}) 146.3 (C_{12}). MS m/z (%): 563 $[M+1]^+$. Λ_M 10^{-3} (ohm^{-1} cm^2 mol^{-1}) = 3.7. λ_{max} (cm^{-1}) in DMF, 42254, 32397. μ_{eff} (BM): diamagnetic.

[ZnL^2Cl_2]. Yield: 58%. Anal. Calc. for $C_{24}H_{22}N_2ZnCl_2$: Zn, 13.8; C, 60.7; H, 4.7; N, 5.9; Found: Zn, 13.7; C, 60.6; H, 4.6; N, 5.9 (%). IR (KBr pellet, cm^{-1}): 1608 ν(–C=N); 1524 ν(–HC=C); 442 (M–N). ^{1}H–NMR (δ, ppm): (aromatic) 6.8–7.2 (m); ($–CH_3$, 6H), 2.2 (s). ^{13}C–NMR (δ, ppm):125.6–128.7 (C_1 to C_3), 133.3 (C_4), 136.1 (C_5), 112.2 (C_6), 168.4 (C_7), 20.2 (C_8), 137.0 (C_9), 119.5 (C_{10}), 131.4 (C_{11}), 128.7 (C_{12}). MS m/z (%): 473 $[M+1]^+$.Λ_M 10^{-3} (ohm^{-1} cm^2 mol^{-1}) = 5.9. λ_{max} (cm^{-1}) in DMF, 40453, 29467. μ_{eff} (BM): diamagnetic.

[ZnL^3Cl_2]. Yield: 54%. Anal. Calc. for $C_{24}H_{22}N_2O_2ZnCl_2$: Zn, 13.0; C, 56.9; H, 4.4; N, 5.5; Found: Zn, 12.9; C, 56.8; H, 4.3; N, 5.5 (%). IR (KBr pellet, cm^{-1}): 1618 ν(–C=N); 1526 ν(–HC=C); 3430 ν(–OH); 445 (M–N). ^{1}H–NMR (δ, ppm): (aromatic) 6.9-7.2 (m); (–OH, 1H) 10.1 (s); ($–CH_3$, 6H), 2.1 (s). ^{13}C–NMR (δ, ppm): 125.1–127.8 (C_1 to C_3), 134.2 (C_4), 136.1 (C_5), 114.1 (C_6), 169.8 (C_7), 20.1 (C_8), 147.4 (C_9), 122.8 (C_{10}), 118.3 (C_{11}), 154.8 (C_{12}). MS m/z (%): 505 $[M+1]^+$. Λ_M 10^{-3} (ohm^{-1} cm^2 mol^{-1}) = 4.5. λ_{max} (cm^{-1}) in DMF, 41567, 33946. μ_{eff} (BM): diamagnetic.

$[ZnL^4Cl_2]$. Yield: 53%. Anal. Calc. for $C_{26}H_{26}N_2O_2ZnCl_2$: Zn, 12.2; C, 58.4; H, 5.0; N, 5.2; Found: Zn, 12.2; C, 58.3; H, 5.0; N, 5.1 (%). IR (KBr pellet, cm^{-1}): 1613 ν(–C=N); 1540 ν(–HC=C); 1267, 1083, ν(–C–O–C–); 433 (M–N). ^{1}H–NMR (δ): (aromatic) 6.8–7.2 (m); (–CH_3, 6H), 2.2 (s); 3.6 (–OCH_3, 6H). ^{13}C–NMR (δ):124.7–128.8 (C_1 to C_3), 132.8 (C_4), 137.2 (C_5), 112.6 (C_6), 167.6 (C_7), 20.5 (C_8), 142.3 (C_9), 122.0 (C_{10}), 116.5 (C_{11}), 158.5 (C_{12}), 58.1 (C_{13}). MS m/z (%): 533 $[M+1]^+$. Λ_M 10^{-3} (ohm^{-1} cm^2 mol^{-1}) = 8.4. λ_{max} (cm^{-1}) in DMF, 42285, 31518. μ_{eff} (BM): diamagnetic.

2.5. DNA binding experiments

The interaction between metal complexes and DNA was studied using electronic absorption, viscosity and electrochemical methods. Disodium salt of calf thymus DNA was stored at 4°C. All the experiments involving the interaction of the complexes with calf thymus (CT) DNA were carried out in Tris–HCl buffer (50 mM Tris–HCl, pH 7.2) containing 5 % DMSO at room temperature. A solution of CT DNA in the buffer gave a ratio of UV absorbance at 260 and 280 nm of about 1.89:1, indicating that the CT DNA was sufficiently free from protein [26]. The concentration of DNA was measured by using its extinction coefficient at 260 nm (6600 $M^{-1}cm^{-1}$) after 1: 100 dilution. Stock solutions were stored at 4°C and used not more than 4 days. Doubly distilled water was used to prepare solutions. Concentrated stock solutions of the complexes were prepared by dissolving the complexes in DMSO and diluting properly with the corresponding buffer to the required concentration for all the experiments.

Absorption titration experiment was performed by keeping the concentration of the metal complex as constant at 50 μM while varying the concentration of the CT DNA within 40–400 μM. While measuring the absorption spectrum, equal quantity of CT DNA was added to both the complex solution and the reference solution to eliminate the absorbance of CT DNA itself. From the absorption data, the intrinsic binding constant (K_b) was determined from the plot of $[DNA]/(\varepsilon_a-\varepsilon_f)$ vs. [DNA] using the equation (1):

$$[DNA]/(\varepsilon_a–\varepsilon_f) = [DNA]/(\varepsilon_b–\varepsilon_f) + [K_b(\varepsilon_b–\varepsilon_f)]^{-1} \text{ ---------- (1)}$$

where [DNA] is the concentration of CT DNA in base pairs. The apparent absorption coefficients ε_a, ε_f and ε_b correspond to A_{obs}./[M], the extinction coefficient for the free metal(II) complex and extinction coefficient for the metal(II) complex in the fully bound form, respectively [27]. K_b is given by the ratio of slope to the intercept.

Cyclic voltammetry studies were performed on a CHI 620C electrochemical analyzer with three electrode system of glassy carbon as the working electrode, a platinum wire as auxiliary electrode and Ag/AgCl as the reference electrode. Solutions were deoxygenated by purging with N_2 prior to measurements. Viscosity experiments were carried on an Ostwald viscometer, immersed in a thermostated water-bath maintained at a constant temperature at 30.0 ± 0.1°C. CT DNA samples of approximately 0.5 mM were prepared by sonicating in order to minimize complexities arising from CT DNA flexibility [28]. Flow time was measured with a digital stopwatch three times for each sample and an average flow time was calculated. Data were presented as $(\eta/\eta_0)^{1/3}$ versus the concentration of the metal(II) complexes, where η is the viscosity of CT DNA solution in the presence of complex, and η_0 is the viscosity of CT DNA solution in the absence of complex. Viscosity values were calculated after correcting the flow time of buffer alone (t_0), $\eta = (t - t_0)/ t_0$ [29].

2.6. Interaction with pBR322 plasmid DNA

The extent of pBR322 DNA cleavage in the absence and presence of an activating agents H_2O_2, groove binding agents, distamycin, methyl green (MG) and SOD (superoxide) radical scavenger was monitored using agarose gel electrophoresis. In reactions using super coiled pBR322 plasmid DNA Form I (2 μL,10 μM) in Tris–HCl buffer (50 mM) with 50 mM NaCl (pH 7.2) which was treated with the metal complex (30 μM) and activating agents (10 μM) followed by dilution with the Tris–HCl buffer to a total volume of 20 μL. The samples were incubated for 1 h at 37 ºC. A loading buffer containing 25% bromophenol blue, 0.35% xylene cyanol, 30% glycerol (3μl) was added and electrophoresis was performed at 40 V for each hour in Tris-Acetate-EDTA (TAE) buffer using 1% agarose gel containing 1.0 μg/mL ethidium bromide. The gel was visualized by photographing the fluorescence of intercalated ethidium bromide under a UV illuminator. The cleavage efficiency was measured by determining the ability of the complex to convert the super coiled (SC) DNA to nicked circular form (NC) and linear form (LC). Inhibition reactions were carried out by prior incubation of the SC pBR322 DNA (40 mM) with DMSO (2 mL).

2.7. Evaluation of antimicrobial activity

Qualitative determination of antimicrobial activity was done using the disc diffusion method. The biological activities of synthesized Schiff base and its metal complexes were

studied for their antibacterial and antifungal activities in DMF solvent against bacterial and fungi species. Suspensions in sterile peptone water from 24 h cultures of microorganisms were adjusted to 0.5 McFarland. Muller–Hinton petri discs of 90 mm were inoculated using these suspensions. Paper discs (6 mm in diameter) containing 10 μL of the substance to be tested were placed in a circular pattern in each inoculated plate. DMF impregnated discs were used as negative controls. Toxicity tests of the solvent, DMF, showed that the concentration used in antibacterial activity assays did not interfere with the growth of the microorganisms.

2.8. Determination of MIC

The *in vitro* antimicrobial activity was performed against Gram-positive bacteria: *Staphylococcous aureus, Bacillus subtilis* and *Salmonella typhi* Gram-negative bacteria: *Escherichia coli, Pseudomonas aeruginosa* and fungal strains: *Rhizoctonia bataticola, Fusarium Solani, Candida albicans, Culvularia lunata* and *Aspergillus niger*. The standard and test samples were dissolved in DMF to give a concentration of 100 μg/mL. The minimum inhibitory concentration (MIC) was determined by broth microdilution method [30]. Dilutions of test and standard compounds were prepared in nutrient broth (bacteria) or Sabouraud dextrose broth (fungi) [31]. The samples were incubated at 37°C for 24 h (bacteria) and at 25°C for 48 h (fungi), respectively, and the results were recorded in terms of MIC (the lowest concentration of test substance which inhibited the growth of microorganisms).

2.9. Antioxidant assays

The ability of all the synthesized complexes to act as free radical scavengers was tested by conducting a series of *in vitro* antioxidant assays involving DPPH radical, hydrogen peroxide, metal chelating assay and the results were compared with that of standard antioxidants including natural antioxidant Vitamin C and synthetic antioxidant BHT (Butylated Hydroxytoluene)..

2.10. DPPH˙ scavenging assay

The DPPH radical scavenging activity of the compounds was measured according to the method of Blios [32]. The DPPH radical is a stable free radical and due to the presence of an odd electron, it shows a strong absorption band at 517 nm in visible spectrum. If this electron becomes paired off in the presence of a free radical scavenger, this absorption vanishes resulting in decolorization stoichiometrically with respect to the number of electrons taken up. Various concentrations of the experimental complexes were taken and the volumes were adjusted to 100

mL with DMSO. About 5 mL of 0.1 mM methanolic solution of DPPH was added to the aliquots of samples and standards (BHT and Vitamin C) and shaken vigorously. Negative control was prepared by adding 100 mL of methanol in 5 mL of 0.1 mM methanolic solution DPPH. The tubes were allowed to stand for 20 min at 27ºC. The absorbance of the sample was measured at 517 nm against the blank (DMSO).

2.11. H_2O_2 scavenging assay

The ability of the complexes to scavenge hydrogen peroxide was determined using the method of Ruch *et al.* [33]. A solution of hydrogen peroxide (2.0 mM) was prepared in phosphate buffer (0.2 M, pH-7.4) and its concentration was determined spectrophotometrically from absorption at 230 nm with molar absorptivity 81 M^{-1} cm^{-1}. The complexes (100 mg/mL), BHT and Vitamin C (100 mg/mL) were added to 3.4 mL of phosphate buffer together with hydrogen peroxide solution (0.6 mL). An identical reaction mixture without the sample was taken as negative control. Absorbance of hydrogen peroxide at 230 nm was determined after 10 min against the blank (phosphate buffer).

2.12. Measurement of SOD like activity

Superoxide dismutase (SOD)-like activity was investigated using Beauchamp and Fridovich's method – as improved by Iwamoto *et al* [34]. This method is based on the inhibitory effect of SOD on the reduction of nitrobluetetrazolium (NBT) by the $O2^{\cdot-}$ generated by the xanthine/xanthine oxidase system. The assay was carried out in the assay buffer containing 50mM Tris HCl, pH 8.0, 0.1 mM DTPA and 0.1 mM hypoxanthine. Radical detector consisted of a tetrazolium salt and was diluted by assay buffer. Similarly, the solutions of SOD standards and xanthine oxidase were prepared in sample buffer consisting of 50mM Tris-HCl, pH 8.0. All the studied complexes were dissolved in DMSO and absorbance was reported for each set of concentrations after 15 min interval. Results were graphed as % inhibition of NBT reduction taken at various concentrations (0 μM-20 μM) for each of the studied complexes. IC_{50} values are reported equivalent concentrations (μM) to 1U bovine erythrocyte superoxide dismutase (native SOD).

2.13. Antitumor studies

Adult Swiss female albino mice (20-25 g) were procured from Animal house, Vivekananda College of Pharmacy, Trichengodu, Tamil Nadu, India and used throughout the

study. They were housed in microlon boxes in controlled environment (temperature 25±2ºC and 12 h dark/light cycle) with standard laboratory diet and water *ad libitum*. The experiments were performed in accordance with guidelines established by the European community for the care and use of laboratory animals, and were approved by the Institutional Animal Ethics Committee (IAEC) of Vivekananda College of Pharmacy, Tamil Nadu, India.

2.14. Cells

Ehrlich Ascites Carcinoma (EAC) cells were obtained through the courtesy of Amala Cancer Research Centre, Trissur, India. They were maintained by weekly intraperitoneal inoculation of 106 cells/mouse [35].

2.15. Mean survival time [36]

Animals were inoculated with 1×10^6 cells/mouse on day '0' and treatment with synthesized complexes started 24 h after inoculation, at a dose of 100 mg/kg/day, p.o. The control group was treated with the same volume of 0.9% sodium chloride solution. All the treatments were given for nine days. The median survival time (MST) of each group, consisting of 10 mice was noted. The antitumor efficacy of complexes was compared with that of 5-fluorouracil (Dabur Pharmaceutical Ltd, India; 5-FU, 20 mg/kg/day, i.p. for 9 days).

2.16. Hematological parameters [36]

The hematological parameters like total red blood cell (RBC), white blood cells (WBC), lymphocytes (LYM), hematocrit (HCT), hemoglobin (HGB) and MID cells (less frequently occurring and rate cells correlating to monocytes, eosinophils, basophils *etc*.) were determined using a blood automatic analyzer (Celldyn, Abbot Inc. USA). In order to detect the influence of complexes on the hematological status of EAC-bearing mice, a comparison was made among three groups (n=5) of mice on the 14th day after inoculation. The groups comprised of (1) tumor-bearing mice (2) tumor-bearing mice treated with complexes (100 mg/kg/day, p.o. for the first 9 days) and (3) control mice (normal). Blood was drawn from each mouse by the retro orbital plexus method and the white blood cell count (WBC), red blood cell count (RBC), hemoglobin and protein were determined [37-40].

2.17. Cytotoxicity

Human cervical cancer cell lines (HeLa), Human laryngeal epithelial cancer (Hep2), Human liver cancer (HepG2) and Human breast cancer (MCF-7) cells were obtained from

National Centre for Cell Science (Pune, India). Stock cells of HeLa, Hep2, HepG2 and MCF-7 cell lines were cultured in RPMI-1640 or DMEM supplemented with 10% in activated new born calf serum, penicillin (100 IU/mL), streptomycin (100 mg/mL), and amphotericin-B (5 mg/mL) under a humidified atmosphere of 5% CO_2 at 37^{o}C until confluent. The cells were dissociated in 0.2% trypsin, 0.02% EDTA in phosphate buffer saline solution. The stock culture was grown in 25 cm^2 tissue-culture flasks, and cytotoxicity experiments were carried out in 96-well microtiter plates (Tarsons India, Kolkata, India).

Cell lines in the exponential growth phase were washed, trypsinized and resuspended in complete culture media. Cells were plated at 10,000 cells / well in 96-well microtiter plates and incubated for 24 h, during which a partial monolayer formed. They were then exposed to various concentrations of the complexes (0.1−100 mg/mL) and cisplatin. Control wells received only maintenance medium. The plates were incubated at 37^{o}C in a humidified incubator with 5% CO_2 for a period of 72 h at the end of 72 h, viability was determined by MTT assay.

3. Results and discussion

Synthetic approaches for the preparation of different biosensitive compounds are depicted in Scheme 1. The ligands and their complexes are found to be stable in air. The ligands are soluble in common organic solvents but their complexes are soluble only in DMF and DMSO.

3.1. Infrared spectra

The coordination mode and sites of the ligand to the metal ions were investigated by comparing the infrared spectra of the free ligand with its metal complexes. The spectra of free ligands show a band in the region 1638-1631 cm^{-1} characteristics of the ν(C=N) stretching mode [41-43] indicating the formation of the Schiff base products. This band is shifted towards lower frequency by *ca.*30 cm^{-1} on complexation compared to free ligands indicating the involvement of the azomethine nitrogen in chelation with the metal ion, the coordination of the nitrogen to the metal ion would be expected to reduce the electron density of the azomethine link and thus causes a shift in the ν(C=N) group [44]. Coupled with this, the absence of a band around 1655–1710 cm^{-1} [45], characteristic of ν(–C=O) in 3-benzylidenepentane-2,4-dione, suggests that the condensation of the keto groups is complete. The free –OH group of the ligand L^3 vibrated at *ca.* 3430 cm^{-1} [45] does not show any significant shift on complex formation. Conclusive evidence of the bonding is also shown by the observation that new bands appear in

the spectra of all metal complexes in the low frequency regions at 420–447 and 360–389 cm^{-1} characteristic for M–N and M–Cl vibrations, respectively, which are not observed in the spectra of free ligands.

3.2. Molar conductivity

The complexes are found to be non-electrolytic nature in 10^{-3} M DMF solution, implying the coordination of chloride anion to the central metal ion. The lower conductance values (3.7–9.2 Ω^{-1} cm^{-2} mol^{-1}) of the complexes support their non-electrolytic nature. The elemental analysis results of the metal complexes also agree with the calculated values, showing that the complexes have 1:1 metal/ligand ratio.

3.3. Magnetic moments and electronic spectra

The geometry of the metal complexes has been deduced from electronic spectra and magnetic data of the complexes. The electronic spectra of the complexes were recorded in DMSO solution. The free ligands exhibit two intense bands in 45857–41656 and 28361-27138 cm^{-1} region due to $\pi \rightarrow \pi^*$ and $n \rightarrow \pi^*$ transitions [46], respectively. In all the metal complexes, the absorption bands at 43928-40263 and 29359-35116 cm^{-1} are due to $\pi \rightarrow \pi^*$ and $n \rightarrow \pi^*$ transitions that are observed in the spectra of the free ligands L^1, L^2, L^3 and L^4. These transitions are shifted to blue or red frequencies due to the coordination of the ligand with metal ions. The electronic spectra of Cu(II) complexes show two broad, low intensity shoulder bands in the visible region, around 17176– 18426 cm^{-1}, which are assigned to the combination of $^2B_{1g} \rightarrow {}^2A_{1g}$ and $^2B_{1g} \rightarrow {}^2E_g$ transitions respectively. The electronic spectral data suggest a square-planar geometry around the Cu(II) ion. The observed magnetic moment of the Cu(II) complexes (1.81-1.87 B.M) at room temperature indicates the non-coupled mononuclear complexes of magnetically diluted d^9 system with S=1/2 spin-state. The monomeric nature of the complexes is further supported by the microanalytical and ESI mass spectral data. The electronic absorption spectra of the diamagnetic Zn(II) complexes show the bands at 40453–42285 and 29467–32946 cm^{-1} which are assigned to intra-ligand charge transfer transitions [47].

3.4. NMR spectra of zinc complexes

In ^1H NMR, the aromatic region is a set of multiplets in the range of 6.8-7.4 ppm for all the ligands and their Zn(II) complexes. The phenolic –OH proton for L^3 ligand and its zinc complex was observed as a singlet at *ca.* 9.3 ppm. It is suggesting that phenolic –OH group is not

taking part in the complexation. ^{1}H NMR spectra of aliphatic methyl protons exhibit at 2.0-2.4 ppm for all the Schiff base ligands and their Zn(II) complexes. There is no appreciable change in all other signals of the complex.

The ^{13}C NMR spectrum of the ligand showed aromatic carbons at 119–129 ppm. The ligand also showed the C=N carbons at 172.8–175.4 ppm, which were shifted to downfield at 167.6–169.2 ppm, upon coordination indicating that the C=N groups participate in complex formation. Comparison of all carbon peaks of the ligands with those of zinc complexes shows some upfield and downfield shifts, but these shifts are not large. This indicates the coordination of the ligand to the metal ion.

3.5. Mass spectra

The ESI-mass spectra of synthesized ligands and their complexes were recorded and the obtained molecular ion peaks confirm the proposed formulae. The mass spectrum of L^1 ligand shows M+1 peak at m/z 428 (86.4 %) corresponding to $[C_{24}H_{20}N_4O_4]^+$ ion. Also, the spectrum exhibits the fragments at m/z 102, 77 and 66 corresponding to $[C_6H_5NO]^+$, $[C_6H_5]^+$ and $[C_5H_6]^+$ respectively. The mass spectrum of $[CuL^1Cl_2]$ shows peaks at m/z 561 with 92.2% abundances, respectively. The strongest peaks (base beak) at m/z 428 represent the stable species $C_{24}H_{20}N_4O_4$. Moreover, the spectrum exhibits the fragments at m/z 102, 77 and 66 corresponding to $[C_6H_5NO]^+$, $[C_6H_5]^+$ and $[C_5H_6]^+$ respectively. The m/z of all the fragments of ligands and their complexes confirm the stoichiometry of the complexes as $[MLCl_2]$. The observed peaks are in good agreement with their formulae as expressed from microanalytical data. Thus, the mass spectral data reinforce the conclusion drawn from the analytical and conductance values.

3.6. EPR spectra

The EPR spectrum of copper complex provides information which is important in studying the metal ion environment. The X-band EPR spectra of all copper(II) complexes have been recorded in DMSO at liquid nitrogen temperature and at room temperature. The spectrum of the copper complexes at RT shows one intense absorption band in the high field and is isotropic due to the tumbling motion of the molecules. However, this complex at LNT shows well resolved peaks with low field region. The spin Hamiltonian parameters of the complexes were calculated and are summarized in Table 1. From this spectral data, it is found that $A_{\|}$ (131-138) > $A_{\perp}$ (39-66); $g_{\|}$ (2.13-2.26) > $g_{\perp}$(2.01-2.05) > g_e 2.0027, which support the $d_{x^2-y^2}$ as

the ground state, characteristic of square-planar geometry and axially symmetric. Further, in an axial symmetry, the g-values are related by the expression,

$$G = (g_{||} - 2.0027)/(g_{\perp}-2.0027)$$

which measures the exchange interaction between the copper centers in polycrystalline solid. The *G* values lie within the range 4.6–5.2 for all the copper complexes indicating negligible exchange interaction of Cu–Cu in the complexes according to Hathaway [48, 49].

For the present copper complexes, the $g_{||}/A_{||}$ values found in the range of 154–174 cm^{-1} are in agreement with significant deviation from planarity which is further confirmed by the bonding parameter α^2 whose value is less than unity.

The covalency parameters α^2 (covalent in-plane σ-bonding) and β^2 (covalent in-plane π-bonding) have been calculated using the following equations [48]. If $\alpha^2 = 1.0$, it indicates complete ionic character whereas $\alpha^2 = 0.5$ denotes 100% covalent bonding, with assumption of negligible small values of the overlap integral.

$$\alpha^2 = (A_{||}/0.036) + (g_{||} - 2.0027) + 3/7\,(g_{\perp} - 2.0027) + 0.04$$

$$\beta^2 = (g_{||} - 2.0027)\,(E / -8\lambda\alpha^2)$$

From Table 1, the α^2 and β^2 values indicate that there is a substantial interaction in the in-plane σ-bonding whereas the in-plane π-bonding is almost ionic. The lower value of α^2 compared to β^2 indicates that the in-plane σ-bonding is more covalent than in-plane π-bonding. These data are well in accordance with other reported values [48]. Based on the above observations, a square-planar geometry is proposed for the complexes. The EPR study of the copper(II) complexes has provided supportive evidence to the conclusion obtained on the basis of electronic and magnetic moment values.

3.7. Electronic absorption titration

The absorption spectra of the ligand $L^1$and its complexes of Cu(II) and Zn(II) in the presence or without DNA were mutually compared, which is shown in Fig. 1a-1c. In the UV region of the spectra, all the ligands exhibited an absorption band around 312.2-323.8 nm (due to π–π* transition) and their copper complexes exhibited an intense absorption around 340–364.5 nm and zinc complexes showed a band at 341.5–369.5 nm (due to n–π* transition). With

increasing concentration of DNA, both the ligands and their complexes showed hypochromicity and a red-shifted charge transfer peak maxima in the absorption spectra. In the case of ligands, Fig. 1a showed hypochromicity in the range 6-8% and slight red-shift in the range 0.3-0.6 nm observed in the absorption spectra. The hypochromicity values of all the complexes observed in the presence of DNA were in the range 6–10%, and their red shifts in the region 0.8–2.0 nm. The change in the absorbance values with increasing amount of DNA was used to evaluate the intrinsic binding constant K_b for the present complexes, the values of which are given in Table 2. The change in hypochromicity may be attributed to the nature of the binding of the complexes with DNA, which is significant due to π-stacking or hydrophobic interactions of the aromatic phenyl rings [50]. However, the metal ions play crucial role in DNA binding by these complexes. The binding strength of the synthesized complexes with DNA is shown as in the following order: $–NO_2$ > –H > –OH > $–OCH_3$. The strong binding affinity of the metal complexes is due to additional π-π interaction through the aromatic phenyl rings and central metal ions as compared with Schiff base ligands. From the results ligands itself act as a pathetic intercalators as compared to complexes which act as strong intercalators. These results suggest that intercalative ligands with extended aromatic plane, good conjugation effect and electron-withdrawing substituted groups can greatly promote the DNA-binding ability of their Knoevenagel condensate complexes.

3.8. Viscosity measurements

The relative specific viscosity of DNA is determined by varying the concentration of the added metal complexes. Measuring the viscosity of DNA is a classical technique used to analyze the DNA binding mode in solution. Under appropriate conditions, intercalation of drugs, such as ethidium bromide [EB], causes a significant increase in the viscosity of a DNA solution due to the increase in the separation of the base pairs of the intercalation sites and hence, results in an increase in the overall DNA contour length, as shown in Fig. 2. The viscosity of the DNA solution increased with increasing ratio of both the copper and zinc complexes to DNA. As expected, the known DNA-intercalator EB increased the relative viscosity of DNA due to its strong intercalation. Compared with EB, complexes exhibit minor increase in the relative viscosity of CT-DNA, suggesting an intercalation mode between the complex and DNA. In case of ligand L^1 exhibits pathetic intercalation, as compared with EB. This result further suggests an

intercalating binding mode of the complexes with DNA and also parallels the above spectroscopic results, such as hypochromism and red shift of the complexes in the presence of DNA. The viscosity studies provide a strong evidence for intercalation. The increase in viscosity of DNA is ascribed to the intercalative binding mode of the drug because this could cause the effective length of the DNA to increase [51].

3.9. Electrochemical studies

Cyclic voltammetric technique provides a useful complement to the previously used methods of investigation like absorption spectral titration and viscosity studies. The cyclic voltammograms of the glassy carbon electrode in solutions containing $[CuL^1Cl_2]$ in the absence and in the presence of varying amounts of DNA are shown in Fig. 3a and 3b. Presence of DNA causes a considerable decrease in the voltammetric current of the redox wave with a slight shift in $E_{1/2}$ to positive potential. The drop of the voltammetric currents in the presence of DNA may be attributed to slow diffusion of the metal complex bound to CT DNA. This in turn indicates the extent of binding affinity of the complex to DNA. The net shift in $E_{1/2}$ can be used to estimate the ratio of equilibrium constants for the binding of 2+ and 1+ ions to DNA. The quasi-reversible redox couples for Cu(II) and Zn(II) complexes in DMF: buffer solution that have been studied upon addition of CT-DNA and the shifts of the cathodic (Epc) and anodic (Epa) potentials are given in Table 3. No new redox peaks appeared after the addition of CT-DNA to each complex, but the current intensity of all the peaks decreased significantly, suggesting the existence of an interaction between each complex and CT-DNA. The decrease in current intensity can be explained in terms of an equilibrium mixture of free and DNA-bound complexes to the electrode surface [52]. Finally, the conclusion derived from the CV study is that copper and zinc complexes can bind to DNA by intercalative binding mode.

3.10. Antimicrobial activity

The minimal inhibitory concentrations of tested compounds against certain bacteria and fungi are shown in Tables 4 and 5. The ligands (L^1–L^4) and their metal complexes were prepared and tested for their *in vitro* antimicrobial activity against the five strains of bacteria (gram negative and gram positive), and five strains of fungi. Few metal complexes of the functionalized β-diketimines showed high *in vitro* antimicrobial activity. All the Cu(II) and Zn(II) metal complexes showed significant antibacterial and antifungal activities compared to free ligands,

But the activity was lesser than the standard drugs. It is clearly depicted in Fig. 4a and 4b. Such increased activity of the complexes can be explained on the basis of Overtone's concept [53] and the Tweedy's Chelation theory [54]. The presence of electron-withdrawing nitro group on the aromatic ring in general increases the antimicrobial activities of the tested metal complexes compared to complexes having no substituent. The nature of metal ion also plays a decisive role in determining antimicrobial properties. In the present study, the order of the antimicrobial activity of the synthesized compounds (based on the substituent present in the phenyl ring) is as follows: $–NO_2$ > –H > $–OCH_3$ > –OH. It is inferred from the results that electron-withdrawing nitro group has effective and direct impact on selective antimicrobial activities against both bacteria and fungi. In the complexes, the ligands have few uncoordinated hetero atoms which enhance the activity of the complexes by bonding with trace elements present in microorganisms may combine with the uncoordinated site and may inhibit the growth of fungi. The mode of action of the compounds may involve the formation of a hydrogen bond through the azomethine group with the active centers of cell constituents, resulting in interferences with the normal cell process [55, 56].

3.11. Cleavage activity of pBR322 plasmid DNA

Gel electrophoresis experiments using pBR322 circular plasmid DNA were performed with the ligands and complexes in the presence and absence of H_2O_2 as an oxidant. At micromolar concentrations for a 2 h incubation period, the ligands exhibited moderate cleavage activity in presence of the oxidant (H_2O_2). The nuclease activity was greatly enhanced by the incorporation of the metal ion into the respective ligands. The cleavage activities of Cu(II) and Zn(II) complexes of β-diketimines on pBR322 DNA are shown in Fig. 5. In Fig. 5, lane 1 is control while the other lanes contain complexes in presence of oxidant (H_2O_2). It is clear that the parent ligands show an apparent cleavage activity in presence of the oxidant. The other lanes contain metal complexes in form I (super coiled) converted into form II (nicked) and form III (linear). The cleavage activity of the complexes is significantly increased in the presence of the oxidant (H_2O_2). This may be attributed to the formation of hydroxyl free radicals, which oxidize +2 to +3, presumably through Fenton-type reactions, resulting in the formation of reactive oxygen species, which could then cause oxidative damage to DNA [57]. In order to clarify the intercalative mechanism of pBR322DNA introduced by metal(II)complexes, the investigation

has been carried out further on adding distamycin and methyl green (groove binders). It is found that no inhibition of DNA cleavage is observed indicating that hydroxyl radical is not involved in the cleavage process in the presence of groove binders (Fig. 6 and Fig. 7). These prompted us to investigate the SOD activity of the metal complexes with pBR322 DNA. While in presence of SOD, a facile superoxide anion radical $O_2^{\bullet-}$ quencher, the cleavage is improved which indicates that $O_2^{\bullet-}$ might be an inhibitor in the cleavage of the plasmid and reducing the amount of $O_2^{\bullet-}$ could improve the cleavage effect (Fig. 8a and 8b). Thus, freely diffusible $OH^{\bullet}$ is considered as the active species responsible for pBR322 DNA cleavage. From these results, we infer that the metal complexes act as potent nuclease agents. As the compounds are observed to cleave the DNA, it can be concluded that, the compound inhibits the growth of the pathogenic organism by cleaving the genome. Therefore, the compounds can be used as promising antitumor agents *in vivo* to inhibit the DNA replication in the cancer cells and not allow the tumor for further growth.

3.12. Anti-oxidative activity

The IC_{50} values of all the complexes (Table 6) obtained from different types of assay experiments strongly support that they possess excellent antioxidant activities, which are better than those of standard antioxidants including the natural antioxidant vitamin C and the synthetic antioxidant BHT (butylated hydroxytoluene). From the results, it is seen that the metal complexes have higher activities than the free ligands due to the presence of the central metal ion moiety in the complexes. At 10 μM concentration, Cu(II) complex of L^1 showed a stronger H_2O_2 scavenging activity (65.5 μM) than other ligands and their complexes. The positive controls, BHT and vitamin C showed 215.3 and 143.6 μM H_2O_2 radical scavenging, respectively. The metal complexes with similar structures showed almost comparable antioxidant activities. Cu(II) complexes, which increase the capacity to stabilize the unpaired electrons and thereby scavenge the free radicals. The hydroxyl radical scavenging power of the tested complexes is the greatest. Being a potent scavenger of hydroxyl radicals, the complexes could capture hydrogen peroxide, as evident from the IC_{50} values [58]. Although the radical scavenging mechanism of the complexes under study remains unclear, the experimental results are helpful in designing more effective antioxidant agents against free radicals.

The DPPH method is described as a simple, rapid and convenient method independent of sample polarity for screening many samples for radical scavenging activity [59]. The DPPH

radical has been widely used to test the ability of compounds as free radical scavengers or hydrogen donors to evaluate the antioxidant activity. The antioxidant activity of complexes is presented in Table 6. At 10 μM concentration, Cu(II) complex of L^1 showed a stronger DPPH scavenging activity (69.6 μM) than other ligands and their complexes. The positive controls, BHT and vitamin C showed 87.4 and 146.8 μM DPPH scavenging, respectively. The marked antioxidant activity of copper complex of L^1, in comparison to free ligands and other complexes, could be due to the coordination of copper in the condensed ring system, increasing its capacity to stabilize unpaired electrons and, thereby, to scavenge free radicals. In addition, incorporation of aromatic moiety in the β-diketone derivatives further enhanced the antioxidant activity. Cu(II) complex of L^1 showed higher antioxidant activity than vitamin C which is due to the introduction of *p*-substituted ($–NO_2$) phenyl moiety in the β-diketimine. It implied that copper complex of L^1 might be considered as new promising lead candidate for further design and synthesis of antioxidants.

3.13. SOD mimetic assay

The $O_2^{\cdot -}$ scavenging activity (IC_{50}) of the complexes was determined by NBT assay using UV-Vis spectroscopy. All Cu(II) complexes demonstrated SOD activity in the micromolar range (IC_{50}) varying from 2.96-7.83 μM as shown in Table 7. Cu(II) Complex (L^1) possesses superior SOD mimetic activity among all the studied complexes. Although, the IC_{50} value of the Cu(II) complex is higher than those reported for native bovine erythrocyte SOD (0.04 μM), it is in good agreement with the IC_{50} values of previously reported synthetic SOD mimics [60,61]. These findings fulfill the prerequisite for complex $[CuL^1Cl_2]$ to act as a potent SOD mimic.

3.14. Antitumor activity against Ehrlich ascite carcinoma cells in mice [62,63]

3.14.1 Effect on biochemical and haematological parameters [62]

On the day 14, the biochemical and haematological parameters, as regard to haemoglobin level, erythrocytes and leucocytes counts, were compared in the group treated with the standard drug 5-FU and the group treated with the newly synthesized Cu(II) compound of L^1, which has shown the highest % increase in lifespan over control, with values obtained from normal and control groups. The EAC tumor cells from the ascitic fluid of different treatment groups were stained with Lieshman stain. They showed marked cytological changes and cytolytic activity when compared to the tumor control cells as shown in Fig. 9a-9c. Similar results were observed

in the present study in animals of the EAC tumor control group. It is found that the cell cycle of normal cells was not affected during the treatment with our complexes whereas the tumor cells were affected in which degenerative changes have been observed in the form of membrane blebbing, vacuolated cytoplasm and a reductive in the staining intensity. As shown in Table 8, the biochemical and haematological parameters in the group treated with the Cu(II) compound of L^1 have been nearly recovered completely to be within the normal values. The values are comparable to those obtained from the group treated with 5-FU.

3.14.2. Effect on survival time

The first measure that can be used to compare the anti-neoplastic activities for the tested compounds is the increase in survival time for each treated group over the control group. The mean survival time (MST) for each group was calculated by dividing the total survival times for all the mice in that group by the number of mice in the same group, then the percent increase in lifespan for each group over the control group was calculated as follows [62]:

$$\%\text{Increase in lifespan over control} = \frac{\text{MST of treated group}}{\text{MST of control group}} \times 100 - 100$$

Comparing the % increase in lifespan of the control group in each treated group (Table 9) revealed that the $[CuL^1Cl_2]$ has shown the same increase in lifespan produced by the standard drug 5-FU. The maximum increase in lifespan was obtained by $[CuL^1Cl_2]$, which nearly cured the animals, expanding their lifespan to be approached to the normal non-diseased group.

3.14.3. Effect of complexes on EAC cell lines

The IC_{50} values of all the synthesized complexes are given in Table 10. This table shows that the complexes demonstrate different anti-tumor activities. The results show excellent potential of $[CuL^1Cl_2]$ complex towards EAC cell lines with IC_{50} value (113.87 μg/mL), very sensitive with the value obtained for the standard drug 5-Flurouracil (5-FU), which is taken as positive control. It suggests that the β-diketimine moiety and its metal ions have important effect on cytotoxicity. Amongst all the complexes tested, $[CuL^1Cl_2]$ has lowest IC_{50} value of 113.87 μg/mL when compared to other complexes. These results indicate that the complexes exert cytotoxic effects against tested carcinoma cell lines.

3.15. Cytotoxicity

A biological assay (MTT assay), which measures the mitochondrial dehydrogenase activity as an indication of cell viability, is carried out. The experiment is performed on four cancer cell lines, HeLa, Hep-2, HepG-2 and MCF-7cells. Cis-Pt$(NH_3)_2Cl_2$ is used as the control, and it shows high cytotoxicity, which is in accordance with the literature reports [64-66]. The Cytotoxicity of complexes is presented in Fig. 10. The IC_{50} values have been calculated after 48 h of incubation with complexes and are listed in Table 11. As shown in Table 11, HeLa and MCF-7cells are more sensitive to Cu(II) complexes of L^1 and L^2 than Hep-G2 and Hep-2 cells, and the cytotoxicities of Cu(II) complex of L^1 against HeLa and MCF-7 cells are higher compared with other complexes and cis-Pt$(NH_3)_2Cl_2$. It is well known that cis-Pt$(NH_3)_2Cl_2$ always displays IC_{50} value in the micromolar range. Although higher complex concentration reduces the percentages of cell survival, there is a significant difference in susceptibility between the complexes and cis-Pt$(NH_3)_2Cl_2$. Due to exist leaving group (chloride ion) in cis-Pt$(NH_3)_2Cl_2$, its cytotoxic effects through covalent binding to DNA form cis-DNA adducts, which interferes with DNA replication and transcription and ultimately induces cell death. According to the results, we speculate that the antitumor activity of all the complexes not only may be related to inserting DNA, but also related to the specific molecular shape of the complex and the chemical structure and nature of the inserted ligand. Synthetically considering these results, the antitumor activity of both complexes are dependent on changing from the parent ligands of electron-withdrawing and electron-releasing substituent at *p*-position, consistent with the affinity of their complexes binding with DNA, and the ability of both complexes effecting on the cells apoptosis are dependent on the values of IC_{50} of complexes against different tumor cell.

4. Conclusion

In this paper, few novel β–diketone derived Schiff bases and their Cu(II) and Zn(II) complexes have been synthesized and characterized by spectral and analytical data. The IR, electronic transition and g tensor data lead to the conclusion that the central metal ion assumes a square planar geometry. The absorption spectroscopy, viscosity measurement and cyclic voltammetry studies have been carried out on the interaction of the complexes with DNA. Comparative DNA binding studies of ligands with their Cu(II) and Zn(II) complexes reveal that the complexes exhibit higher binding affinity towards DNA as compared to ligands. The Cu(II)

complex of L^1 shows the highest binding affinity. The plasmid pBR322 DNA cleavage activity of the complexes is significantly increased in the presence of the oxidant (H_2O_2). No inhibition of DNA cleavage is observed indicating that hydroxyl radical is not involved in the cleavage process in the presence of groove binders which confirms the intercalative mode of binding. We have evaluated *in vitro* the antibacterial, antifungal and antioxidant activities of newly synthesized Schiff base ligands and their metal complexes. The copper(II) complex of L^1 has higher potency against Gram-positive bacteria than Gram-negative bacteria. Copper may easily interact with radicals, especially with molecular oxygen. Enzymatic behavior fulfills the prerequisite for complex $[CuL^1Cl_2]$ to act as a potent SOD mimic. Mononuclear Cu(II) and Zn(II) complexes together with β–diketimine ligands are tested against several human tumor cells which reveal significant antitumor activity and lower resistance of tumor cells *in vitro* than cisplatin. The results suggest that all the complexes produce a potent antitumor and cytotoxic effect against EAC.

Acknowledgements

The authors express their heartfelt thanks to the Science & Engineering Research Board (SERB), DST, New Delhi for financial Support. They also express their gratitude to the College Managing Board, Principal and Head of the Department of Chemistry, VHNSN College, Virudhunagar for providing research facilities. They thank Prof. R. Senthil Kumar, Department of Pharmaceutical Chemistry, Swami Vivekanandha College of Pharmacy, Elayampalayam, Tiruchengodu, for *in vitro* and *in vivo* anti-cancer studies.

.

References

[1] A.W. Prestayko, S.T. Crooke, S.K. Carter, University of Alabama in Birmingham, Comprehensive Cancer, Academic Press, L. Bristol, New York, 1980.

[2] R.B. Weiss, M.C. Christian, Drugs 46 (1993) 360–377.

[3] M. Gordon, S. Hollander, J. Med. 24 (1993) 209–265.

[4] E.R. Jamieson, S.J. Lippard, Chem. Rev. 99 (1999) 2467–2498.

[5] D.D. Von Hoff, R. Schilsky, C.M. Reichert, R.L. Reddick, M. Rozencweig, R.C. Young, F.M. Muggia, Cancer Treat. Rep. 63 (1979) 1527–1531.

[6] P.J. Loehrer Sr., S.D. Williams, L.H. Einhorn, J. Natl, Canc. Inst. 80 (1988) 1373–1382.

[7] M. Coluccia, G. Natalie, Anti Canc. Agents Med. Chem. 7 (2007) 111–123.

[8] P. Heffeter, U. Jungwirth, M. Jakupec, C. Hartinger, M. Galanski, L. Elbling, M. Micksche, B. Keppler, W. Berger, Drug Resist. Updat. 11 (2008) 1–16.

[9] P. Krishnamoorthy, P. Sathyadevi, A. H. Cowley, R. R. Butorac, N. Dharmaraj, Eur. J. Med. Chem. 46 (2011) 3376-3387.

[10] F. Arjmand, A. Jamsheera, D.K. Mohapatra, J. Photochem. Photobiol. 121B (2013) 75-85

[11] H. Liu, X. Shi, M. Xu, Z. Li, L. Huang, D. Bai, Z.Z. Zeng, Eur. J. Med. Chem. 46 (2011) 1638-1647.

[12] W. Szczepanik, J. Ciesiolka, J. Wrzesinski, J. Skala, M. Jezowska-Bojczuk, Dalton Trans. (2003) 1488–1494.

[13] J.P. Annaraj, K.M. Ponvel, P.R. Athappan, Transition Met. Chem., 29 (2004) 722-727.

[14] S. Srinivasan, G. Rajagopal, P.R. Athappan, Transition Met. Chem., 26 (2001) 588-593.

[15] D.J. Bray, J.K. Clegg, L.F. Lindoy, D. Schilter, Adv. Inorg. Chem. 59 (2007) 1–37.

[16] G. Aromi, P. Gamez, J. Reedik, Coord. Chem. Rev. 252 (2008) 964–989.

[17] P. A. Vigato, V. Peruzzo, S. Tamburini, Coord. Chem. Rev. 253 (2009) 1099–1201.

[18] I.A. Hemmila, Applications of Fluorescence in Immunoassays, Wiley, New York, 1991.

[19] N. Sabbatini, M. Guardigli, J.M. Lehn, Coord. Chem. Rev. 123 (1993) 201–228.

[20] Z. Chen, W. Yiqun, F. Huang, G. Donghong, F. Gan, Spectrochim. Acta 66A (2007) 1024–1029.

[21] R. Karvembu, K. Natarajan, Polyhedron 21 (2002) 219–223.

[22] H. Zeng, J. Xie, P.G. Schultz, Bioinorg. Med. Chem. Lett. 16 (2006) 5356–5359.

[23] M.S.A. Begum, S. Saha, A. Hussain, A.R. Chakravarty, Indian J.Chem. 48A (2009) 9–14.

[24] N. Raman, L. Mitu, A. Sakthivel, M.S.S. Pandi, J. Iran. Chem. Soc. 6 (2009) 738–748.

[25] M. Yamamoto, Y. Watanabe, T. Mitsudo, Y. Nakagami, Bull. Chem. Soc. Jpn. 51 (1978) 835-838.

[26] J.Marmur, J. Mol. Biol. 3 (1961) 208-218.

[27] L.F. Tan, X.H. Liu, H. Chao, L.N. Ji, J. Inorg. Biochem. 101 (2007) 56-63.

[28] J.B. Charies, N. Dattagupta, D.M. Crothers, Biochemistry 21 (1982) 3933-3937.

[29] S. Satyanarayanan, J.C. Davorusak, J.B. Charies, Biochemistry 32 (1983) 2573-2584.

[30] M. Sonmez, M. Celebi, I. Berber, Eur. J. Med. Chem. 45 (2010) 1935–1940.

[31] R. Senthil Kumar, S. Arunachalam, Polyhedron 26 (2007) 3255–3262.

[32] M.S. Blois, Nature 26 (1958) 1199-1200.

[33] R.J. Ruch, S.J. Cheng, J.E. Klaunig, Carcinogen. 10 (1989) 1003-1008.

[34] Y. Iwamoto, J. Mifuchi, Chem. Pharm. Bull. 30 (1982) 237-241.

[35] B.G. Tweedy, Phytopathology 55 (1964) 910-914.

[36] B.D. Clarkson, J.H. Burchenal, Prog. Clin. Cancer. 1 (1965) 625-629.

[37] N. Raman, R. Jeyamurugan, R. Senthilkumar, B. Rajkapoor, S.G. Franzblau, Eur. J. Med. Chem. 45 (2010) 5438-5451.

[38] F.F. D.Amour, F.R. Blood, D.A. Belden, The Manual for Laboratory Work in Mammalian Physiology. The University of Chicago Press, Chicago (1965) 23-24.

[39] O.H. Lowry, N.T. Rosenbrough, A.L. Farr, R.J. Randall, J. Biol. Chem. 193 (1951) 265-275.

[40] J.V. Docie, Practical Hematology, 2nd ed. J&A Churchill Ltd., London (1958) 38-42.

[41] C.G. Mohamed, Z.H.A. El-Wahab, J. Therm. Calorim., 73 (2003) 347-359.

[42] P.B. Sreeja, M.R.P. Kurup, Spectrochim. Acta, 61A (2005) 331-336.

[43] C. Jayabalakrishnan, K. Natarajan, Transition Met. Chem., 27 (2002) 75-79.

[44] Z.H.A. El-Wahab, M.M. Mashaly, A.A. Salman, B.A. El-Shetary, A.A. Faheim, Spectrochim. Acta, 60A (2004) 2861-2873.

[45] N. Raman, R. Jeyamurugan, B. Rajkapoor, L. Mitu, J. Iran. Chem. Soc. 7 (2010) 917-933.

[46] A.B.P. Lever, Inorganic Electronic Spectroscopy, Elsevier, Amesterdam, (1984).

[47] A.W. Addison, Inorg. Chim. Acta, 162 (1989) 217-220.

[48] R.K. Ray, G.B. Kauffman, Inorg. Chim. Acta, 173 (1990) 207-214.

[49] N. Raman, R. Jeyamurugan, J. Coord. Chem., 62 (2009) 2375-2387.

[50] N. Shahabadi, M. Falsafi, N.H. Moghadam, J. Photochem. Photobiol. 122B (2013) 45-51.

[51] M.C. Prabahara, H.S. Bhojya Naik, Biometals 21 (2008) 675-684.

[52] S. Tabassum, S. Parveen, F. Arjmand, Acta Biomater., 1 (2005) 677-689.

[53] R. Ramesh, S. Maheswaran, J. Inorg. Biochem. 96 (2003) 457–462.

[54] Y. Anjaneyulu, R.P. Rao, Synth.React.Inorg.-Org.Chem. 16 (1986) 257-272.

[55] A.S. Munde, A.N. Jagdale, S.M. Jadhow, T.K. Chondhekar, J. Korean Chem. Soc., 53 (2009) 407-410.

[56] N. Raman, R. Jeyamurugan, M. Subbulakshmi, R. Boominathan, C.R. Yuvarajan, Chem. Pap. 64 (2010) 378-385.

[57] R. B. Nair, E. S. Teng, S. L. Kirkland, C. J. Murphy, Inorg. Chem. 37 (1998) 139-141.

[58] K. Tsai, T. G. Hsu, K. M. Hsu, H. Cheng, T. Y. Liu, C. F. Hsu, C. W. Kong, Free Radical Biol. Med. 31 (2001)1465–1472.

[59] B. Halliwell, Am. J. Med. 91(1991)14–22.

[60] G. Lupidi, F. Marchetti, N. Masciocchi, D.L. Reger, S. Tabassum, P. Astolfi, E. Damiani, C. Pettinari, J. Inorg. Biochem. 104 (2010) 820-830.

[61] K. Ghosh, V.Mohan, P. Kumar, U.P. Singh, Polyhedron 49 (2013) 167-176.

[62] M. Gupta, U.K. Mazumder, N. Rath, D.K. Mukhopadhyay, J. Ethnopharmacol. 72 (2000) 151-156.

[63] S. Qureshi, O.A. Al-Shabanah, M.M. Al-Harbi, A.M. Al-Bekairi, M. Raza, Toxicology 165 (2001) 1-11;

[64] T.F.S. Silva, L.M.D.R. S. Martins, M. F. C. G. Silva, A.R. Fernandes, A. Silva, P.M. Borralho, S. Santos, C.M.P. Rodrigues, A.J. L. Pombeiro, Dalton Trans. 41 (2012) 12888-12897.

[65] C. Icsel, V.T. Yilmaz, F. Ari, E. Ulukaya, W.T.A. Harrison, Eur. J. Med. Chem. 60 (2013) 386-394.

[66] B. Fei, W. Li, W.S. Xu, Y.G. Li, J.Y. Long, Q.B. Liu, K.Z. Shao, Z.M. Su, W.Y. Sun, J. Photochem. Photobiol. 125B (2013) 32-41.

Figure Captions

Scheme 1. Synthesis of Schiff base ligands and their metal complexes.

Fig. 1a. Absorption spectrum of ligand L^1 in buffer pH = 7.2 at 25 ^{0}C in presence of increasing amount of DNA.

Fig. 1b. Absorption spectrum of $[CuL^1Cl_2]$ in buffer pH = 7.2 at 25 ^{0}C in presence of increasing amount of DNA.

Fig. 1c. Absorption spectrum of $[ZnL^1Cl_2]$ in buffer pH = 7.2 at 25 ^{0}C in presence of increasing amount of DNA.

Fig. 2. Effect of increasing amounts of [EB] (■), $[CuL^1Cl_2]$ (♦), $[CuL^2Cl_2]$ (●), $[CuL^3Cl_2]$ (▲), $[CuL^4Cl_2]$ (■), $[ZnL^1Cl_2]$ (●), $[ZnL^2Cl_2]$ (ж), $[ZnL^3Cl_2]$ (▲), $[ZnL^4Cl_2]$ (■) and [L1] (♦) on the relative viscosity of DNA.1/R = [Complex]/[DNA] or [EB]/[DNA].

Fig. 3a. Cyclic voltammogram of $[ZnL^1Cl_2]$ in buffer pH = 7.2 at 25 ^{0}C in presence of increasing amount of DNA.

Fig. 3b. Cyclic voltammogram of $[CuL^1Cl_2]$ in buffer pH = 7.2 at 25 ^{0}C in presence of increasing amount of DNA.

Fig. 4a. Minimum inhibitory concentration of the synthesized compounds against the growth of bacteria (μg/mL).

Fig. 4b. Minimum inhibitory concentration of the synthesized compounds against growth of fungi (μg/mL).

Fig. 5. Gel electrophoresis pattern showing cleavage of pBR322 supercoiled DNA (10 μM) by complexes Cu(II) and Zn(II). Lane 1: DNA alone; lane 2: 60 μM [L^1] + DNA + H_2O_2; lane 3: 60 μM $[CuL^1Cl_2]$ + DNA + H_2O_2; lane 4: 60 μM $[CuL^2Cl_2]$ + DNA +H_2O_2; lane 5: 60 μM $[CuL^3Cl_2]$ + DNA + H_2O_2; lane 6: 60 μM $[CuL^4Cl_2]$ + DNA + H_2O_2; lane 7: 60 μM $[ZnL^1Cl_2]$ + DNA + H_2O_2; lane 8: 60 μM $[ZnL^2Cl_2]$ + DNA + H_2O_2; lane 9: 60 μM $[ZnL^3Cl_2]$ + DNA + H_2O_2; lane 10: 60 μM $[ZnL^4Cl_2]$ + DNA + H_2O_2.

Fig. 6. Agarose gel electrophoresis pattern showing the cleavage of pBR322 (10μM) plasmid DNA (10 μM) by complexes 60 μM in presence of DNA minor groove binding agent distamycin (100 μM) at 310 K after incubation for 30 min. Lane 1: DNA alone; lane 2: 60 μM $[CuL^1Cl_2]$ + DNA + distamycin; lane 3: 60 μM $[CuL^2Cl_2]$ + DNA +distamycin; lane 4: 60 μM $[CuL^3Cl_2]$ + DNA + distamycin; lane 5: 60 μM $[CuL^4Cl_2]$ + DNA + distamycin; lane 6: 60 μM $[ZnL^1Cl_2]$ + DNA + distamycin; lane 7: 60 μM

$[ZnL^2Cl_2]$ + DNA + distamycin; lane 8: 60 μM $[ZnL^3Cl_2]$ + DNA + distamycin; lane 9: 60 μM $[ZnL^4Cl_2]$ + DNA + distamycin.

Fig. 7. Agarose gel electrophoresis pattern showing the cleavage of pBR322 (10μM) plasmid DNA (10 μM) by complexes 60 μM in presence of DNA major groove binding agent methyl green (MG) (2.5 mL of a 0.01 μg/mL solution) at 310 K after incubation for 30 min. Lane 1: DNA alone; lane 2: 60 μM $[CuL^1Cl_2]$ + DNA + MG; lane 3: 60 μM $[CuL^2Cl_2]$ + DNA + MG; lane 4: 60 μM $[CuL^3Cl_2]$ + DNA + MG; lane 5: 60 μM $[CuL^4Cl_2]$ + DNA + MG; lane 6: 60 μM $[ZnL^1Cl_2]$ + DNA + MG; lane 7: 60 μM $[ZnL^2Cl_2]$ + DNA + MG; lane 8: 60 μM $[ZnL^3Cl_2]$ + DNA + MG; lane 9: 60 μM $[ZnL^4Cl_2]$ + DNA + MG.

Fig. 8a. Gel electrophoresis pattern showing cleavage of pBR322 supercoiled DNA (10 μM) by Cu(II) complexes of L^1-L^4 in presence of SOD (1U). Lane 1: DNA alone; lane 2: 60 μM $[CuL^1Cl_2]$ + DNA + SOD (1U); lane 3: 60 μM $[CuL^2Cl_2]$ + DNA + SOD (1U); lane 4: 60 μM $[CuL^3Cl_2]$ + DNA + SOD (1U); lane 5: 60 μM $[CuL^4Cl_2]$ + DNA + SOD (1U);

Fig. 8b. Gel electrophoresis pattern showing cleavage of pBR322 supercoiled DNA (10 μM) by Zn(II) complexes of L^1-L^4 in presence of SOD (1U). Lane 1: DNA alone; lane 2: 60 μM $[ZnL^1Cl_2]$ + DNA + SOD (1U); lane 3: 60 μM $[ZnL^2Cl_2]$ + DNA + SOD (1U); lane 4: 60 μM $[ZnL^3Cl_2]$ + DNA + SOD (1U); lane 5: 60 μM $[ZnL^4Cl_2]$ + DNA + SOD (1U).

Fig. 9a. Smear showing matured EAC control cells with definite cell wall and structure without degeneration.

Fig. 9b. EAC tumor cells showing degenerative changes in the form of membrane blebbing, cell wall fragmentation and low staining intensity.

Fig. 9c. Cu(II) complex of L^1 treated EAC Cells showing degenerative changes like membrane blebbing, vacuolated cytoplasm and low staining intensity with complete destruction of cells.

Fig. 10. IC_{50} (mg/mL) values of complexes and cisplatin against various cancer cell lines.

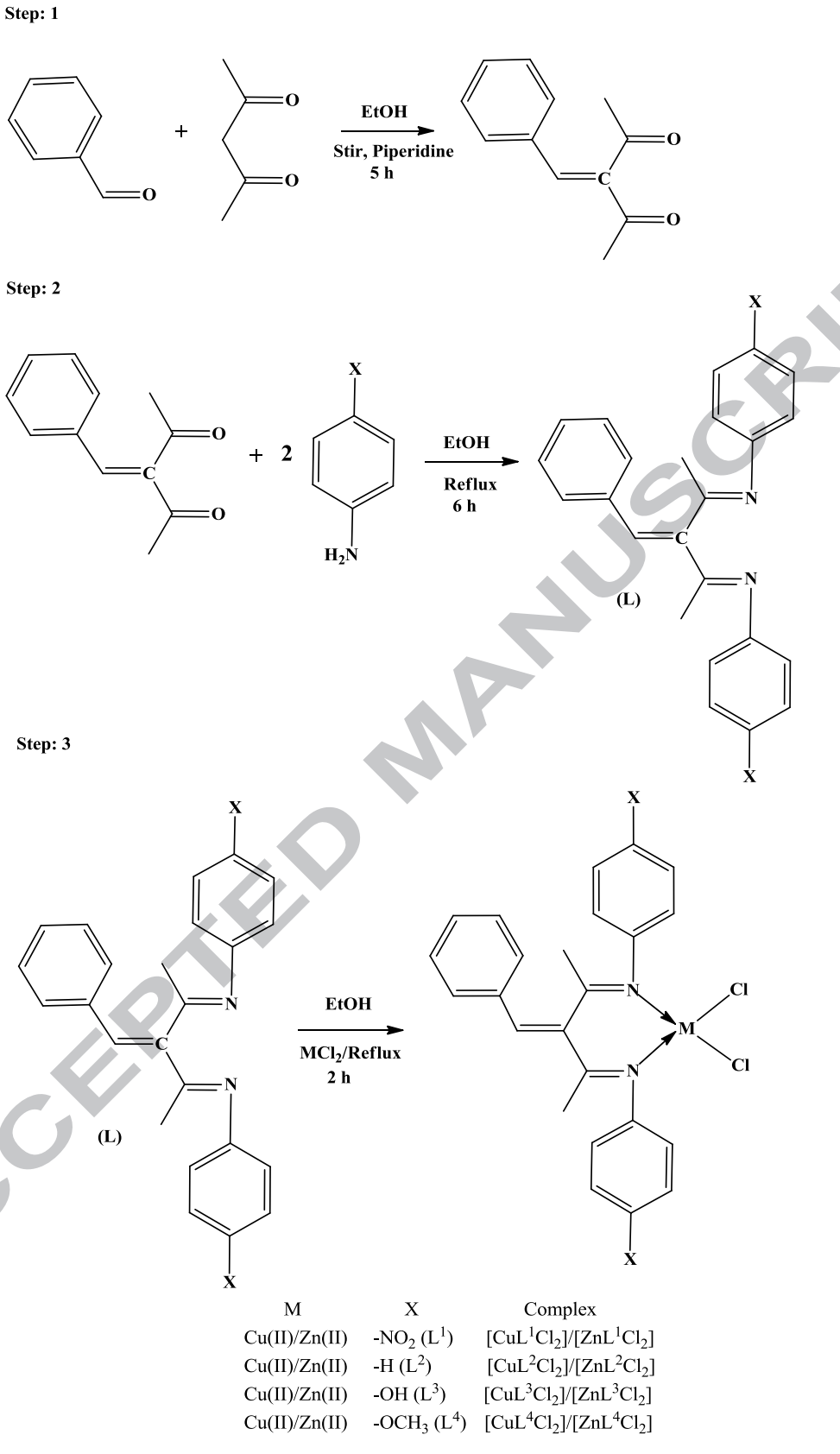

Scheme 1. Synthesis of Schiff base ligands and their metal complexes

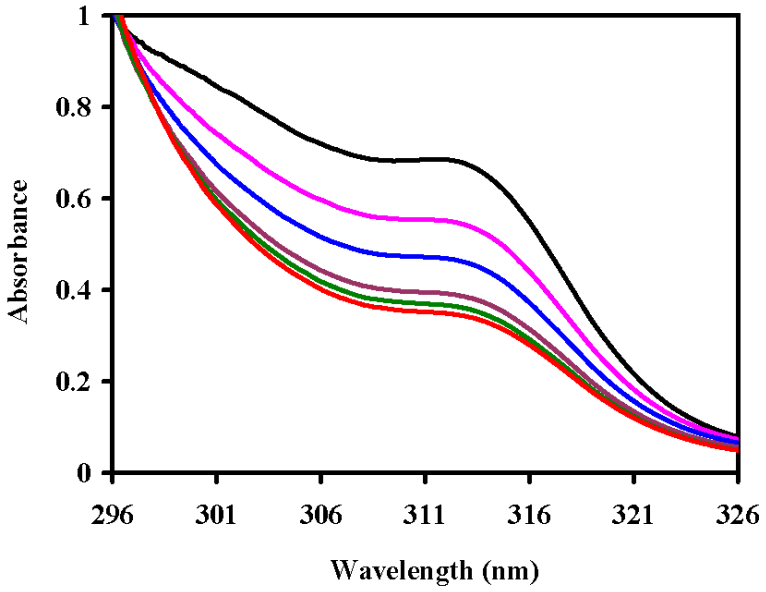

Fig. 1a. Absorption spectrum of ligand L^1 in buffer pH = 7.2 at 25 ^{0}C in presence of increasing amount of DNA.

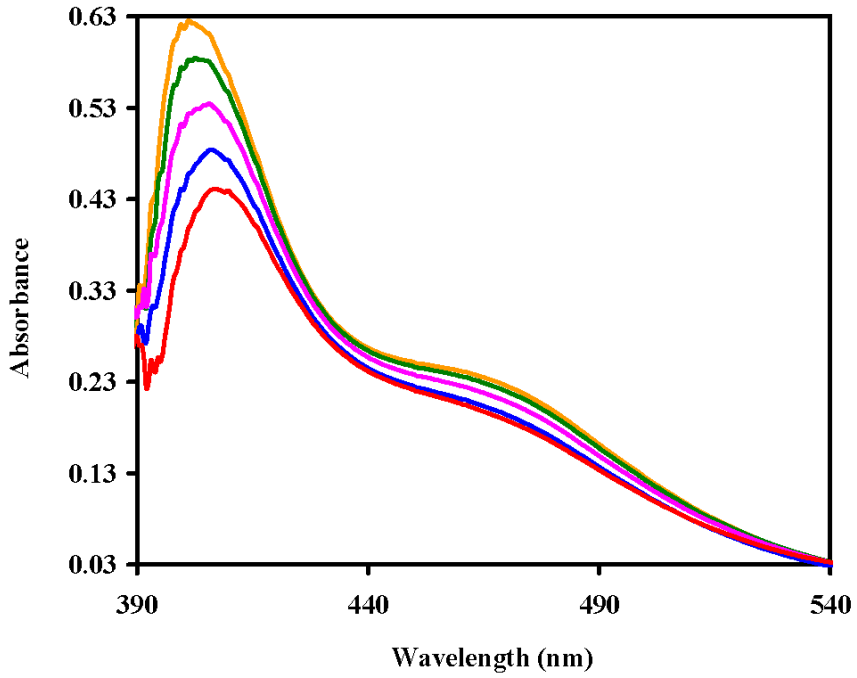

Fig. 1b. Absorption spectrum of $[CuL^1Cl_2]$ in buffer pH = 7.2 at 25 ^{0}C in presence of increasing amount of DNA.

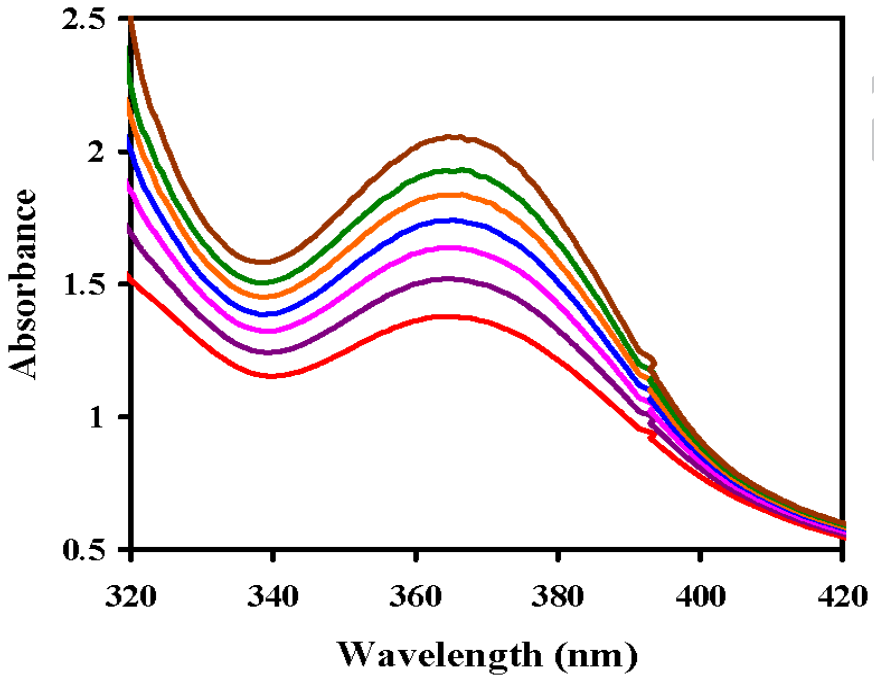

Fig. 1c. Absorption spectrum of $[ZnL^1Cl_2]$ in buffer pH = 7.2 at 25 ^{0}C in presence of increasing amount of DNA.

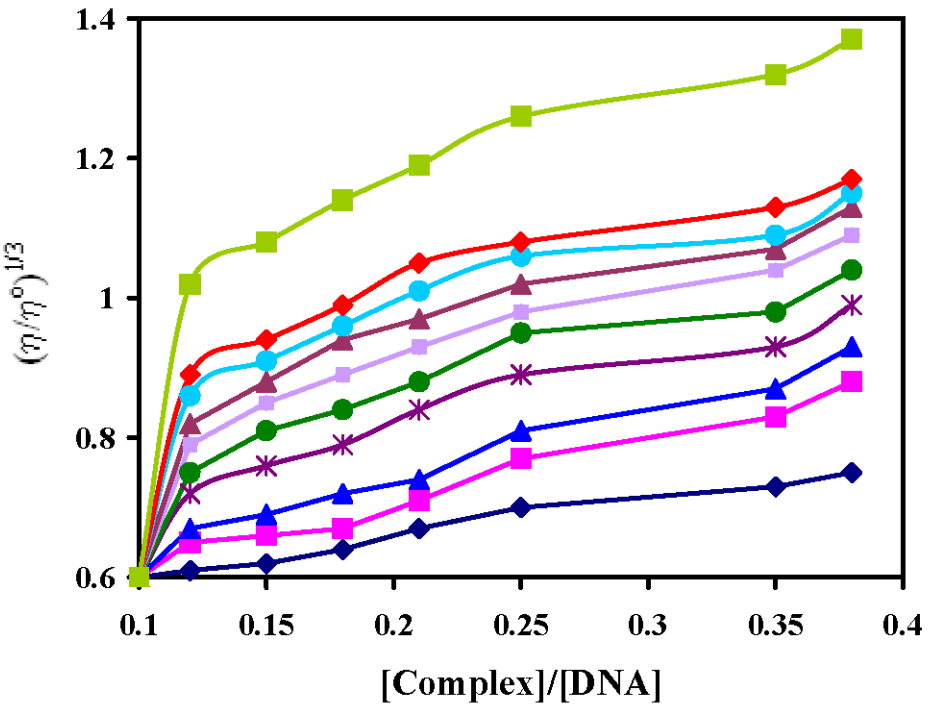

Fig. 2. Effect of increasing amounts of [EB] (■), [CuL^1Cl_2] (♦), [CuL^2Cl_2] (●), [CuL^3Cl_2] (▲), [CuL^4Cl_2] (▪), [ZnL^1Cl_2] (●), [ZnL^2Cl_2] (ж), [ZnL^3Cl_2] (▲), [ZnL^4Cl_2] (▪) and [L1] (♦) on the relative viscosity of DNA.1/R = [Complex]/[DNA] or [EB]/[DNA].

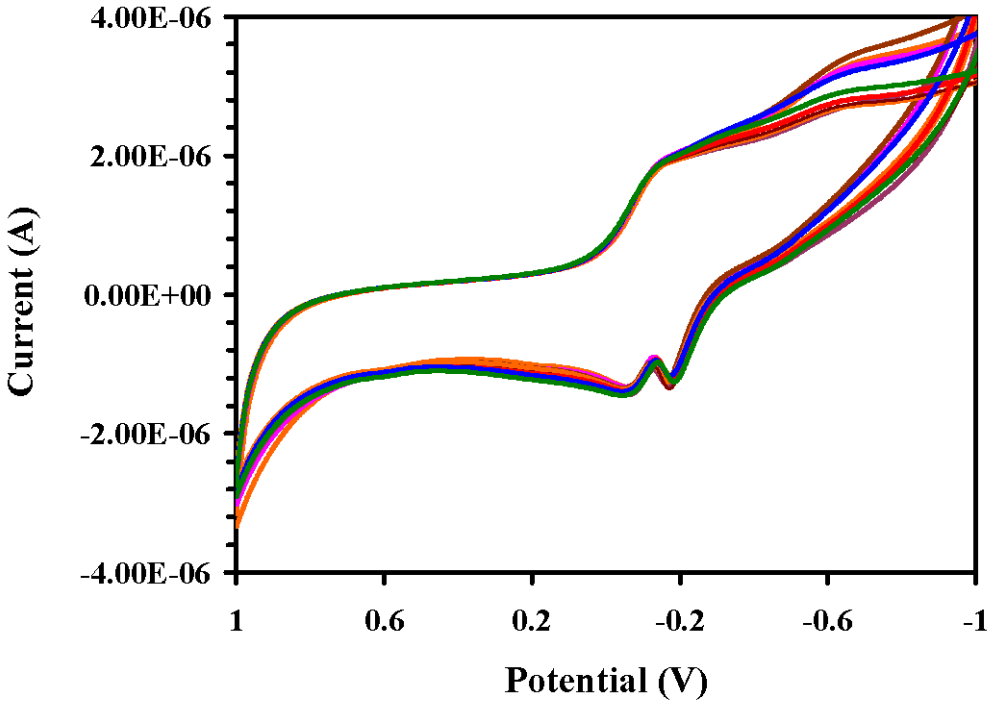

Fig. 3a. Cyclic voltammogram of [ZnL^1Cl_2] in buffer pH = 7.2 at 25 ^{0}C in presence of increasing amount of DNA.

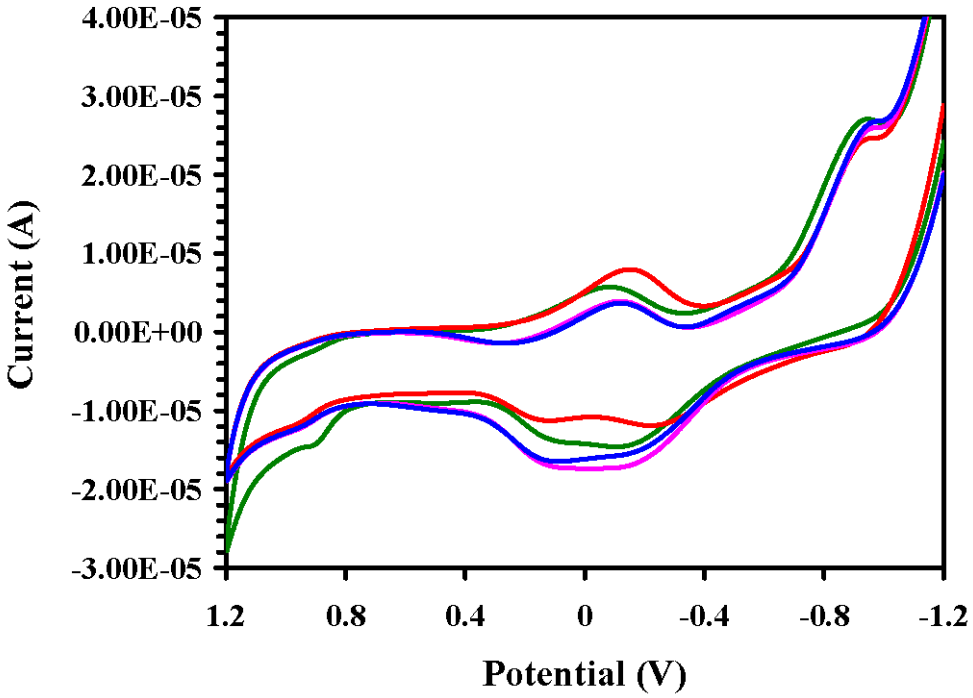

Fig. 3b. Cyclic voltammogram of $[CuL^1Cl_2]$ in buffer pH = 7.2 at 25 ^{0}C in presence of increasing amount of DNA.

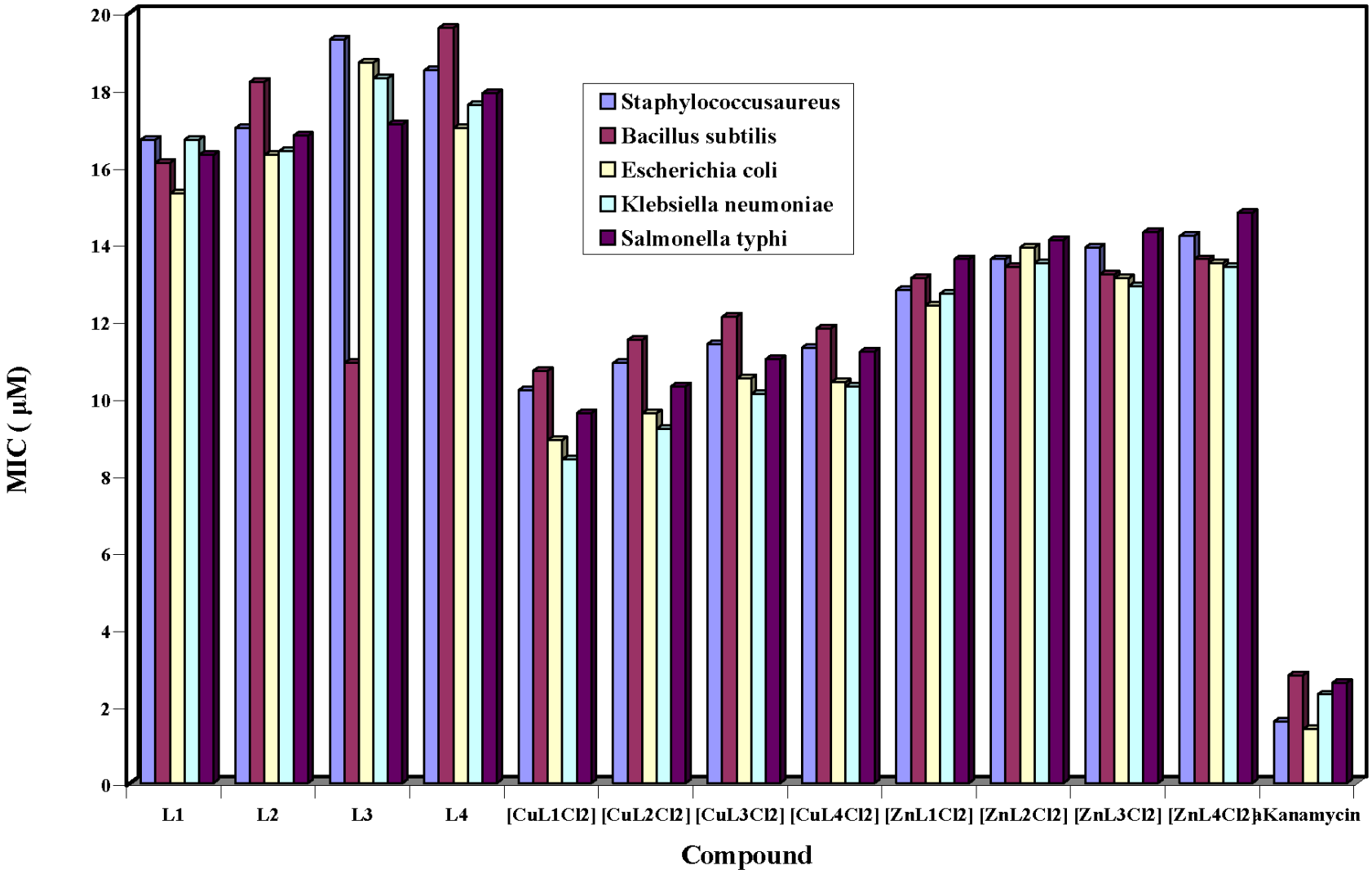

Fig. 4a. Minimum inhibitory concentration of the synthesized compounds against the growth of bacteria (µM)

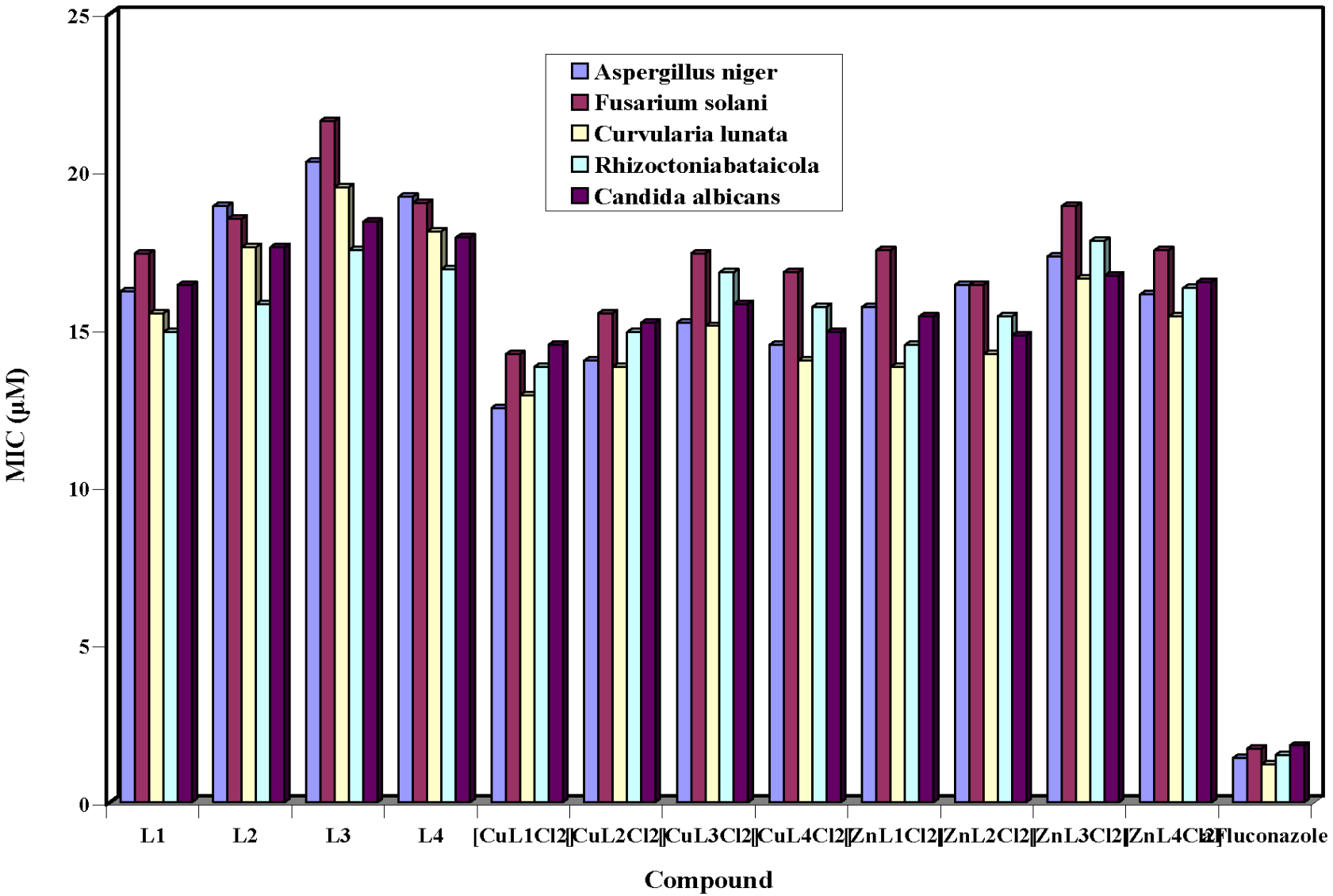

Fig. 4b. Minimum inhibitory concentration of the synthesized compounds against the growth of fungi (µM)

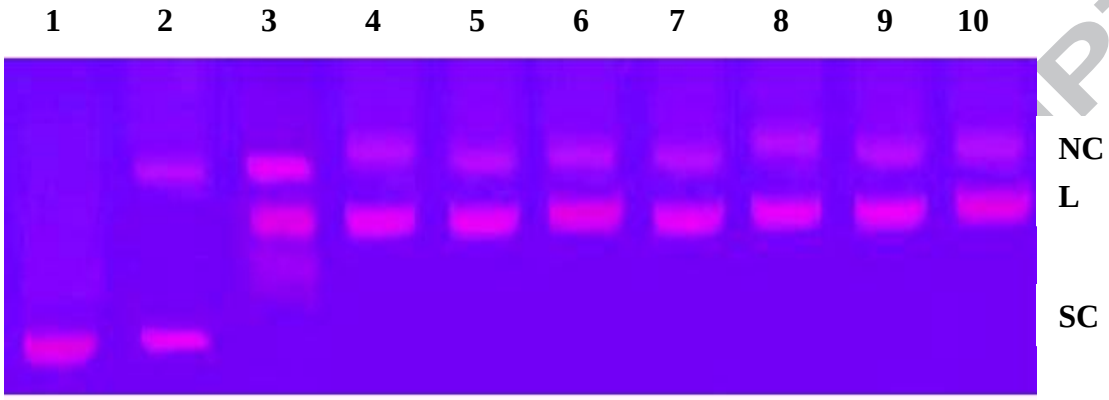

Fig. 5. Gel electrophoresis pattern showing cleavage of pBR322 supercoiled DNA (10 μM) by complexes Cu(II) and Zn(II). Lane 1: DNA alone; lane 2: 60 μM [L^1] + DNA + H_2O_2; lane 3: 60 μM [CuL^1Cl_2] + DNA + H_2O_2; lane 4: 60 μM [CuL^2Cl_2] + DNA +H_2O_2; lane 5: 60 μM [CuL^3Cl_2] + DNA + H_2O_2; lane 6: 60 μM [CuL^4Cl_2] + DNA + H_2O_2; lane 7: 60 μM [ZnL^1Cl_2] + DNA + H_2O_2; lane 8: 60 μM [ZnL^2Cl_2] + DNA + H_2O_2; lane 9: 60 μM [ZnL^3Cl_2] + DNA + H_2O_2; lane 10: 60 μM [ZnL^4Cl_2] + DNA + H_2O_2.

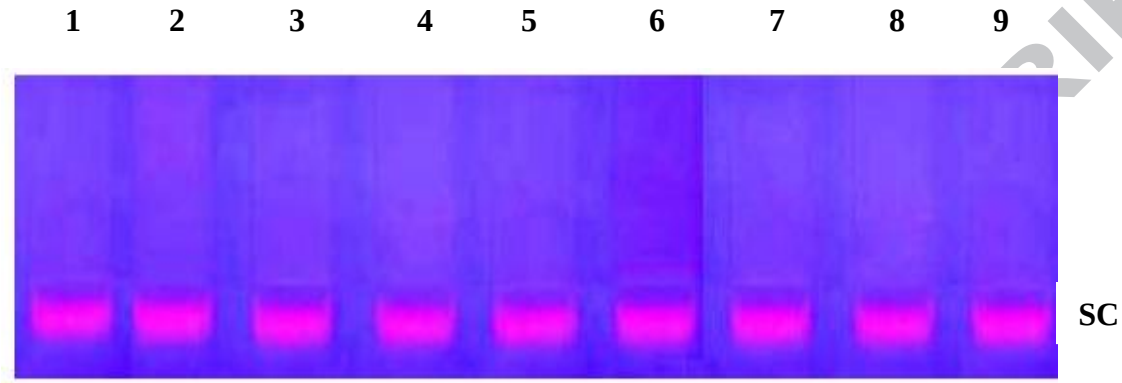

Fig. 6. Agarose gel electrophoresis pattern showing the cleavage of pBR322 (10μM) plasmid DNA (10 μM) by complexes 60 μM in presence of DNA minor groove binding agent distamycin (100 μM) at 310 K after incubation for 30 min. Lane 1: DNA alone; lane 2: 60 μM [CuL^1Cl_2] + DNA + distamycin; lane 3: 60 μM [CuL^2Cl_2] + DNA +distamycin; lane 4: 60 μM [CuL^3Cl_2] + DNA + distamycin; lane 5: 60 μM [CuL^4Cl_2] + DNA + distamycin; lane 6: 60 μM [ZnL^1Cl_2] + DNA + distamycin; lane 7: 60 μM [ZnL^2Cl_2] + DNA + distamycin; lane 8: 60 μM [ZnL^3Cl_2] + DNA + distamycin; lane 9: 60 μM [ZnL^4Cl_2] + DNA + distamycin.

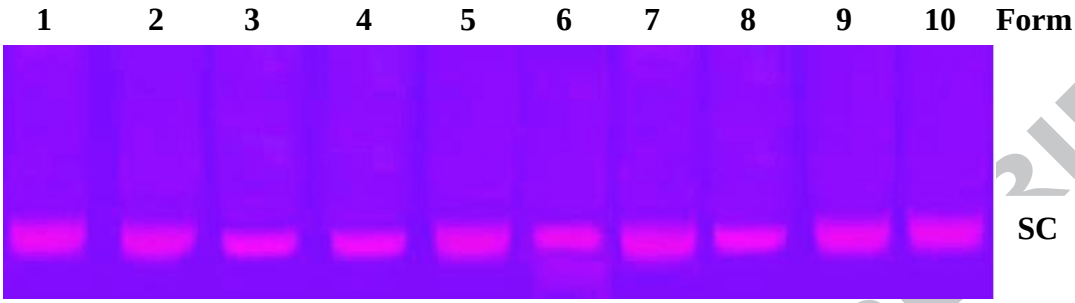

Fig. 7. Agarose gel electrophoresis pattern showing the cleavage of pBR322 (10μM) plasmid DNA (10 μM) by complexes 60 μM in presence of DNA major groove binding agent methyl green (MG) (2.5 mL of a 0.01 μg/mL solution) at 310 K after incubation for 30 min. Lane 1: DNA alone; lane 2: 60 μM $[CuL^1Cl_2]$ + DNA + MG; lane 3: 60 μM $[CuL^2Cl_2]$ + DNA + MG; lane 4: 60 μM $[CuL^3Cl_2]$ + DNA + MG; lane 5: 60 μM $[CuL^4Cl_2]$ + DNA + MG; lane 6: 60 μM $[ZnL^1Cl_2]$ + DNA + MG; lane 7: 60 μM $[ZnL^2Cl_2]$ + DNA + MG; lane 8: 60 μM $[ZnL^3Cl_2]$ + DNA + MG; lane 9: 60 μM $[ZnL^4Cl_2]$ + DNA + MG.

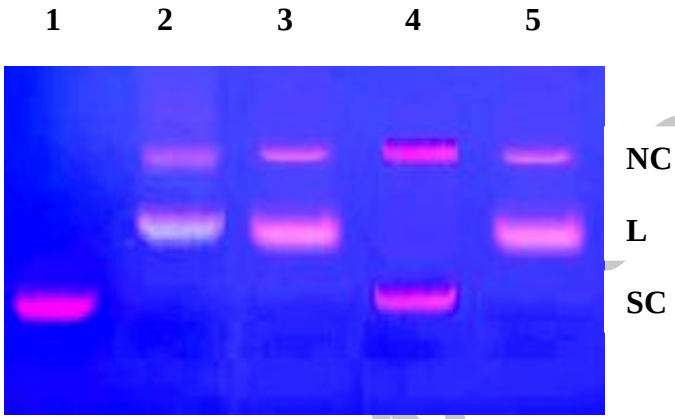

Fig. 8a. Gel electrophoresis pattern showing cleavage of pBR322 supercoiled DNA (10 μM) by Cu(II) complexes of L^1-L^4 in presence of SOD (1U). Lane 1: DNA alone; lane 2: 60 μM [CuL^1Cl_2] + DNA + SOD (1U); lane 3: 60 μM [CuL^2Cl_2] + DNA + SOD (1U); lane 4: 60 μM [CuL^4Cl_2] + DNA + SOD (1U); lane 5: 60 μM [CuL^3Cl_2] + DNA + SOD (1U);

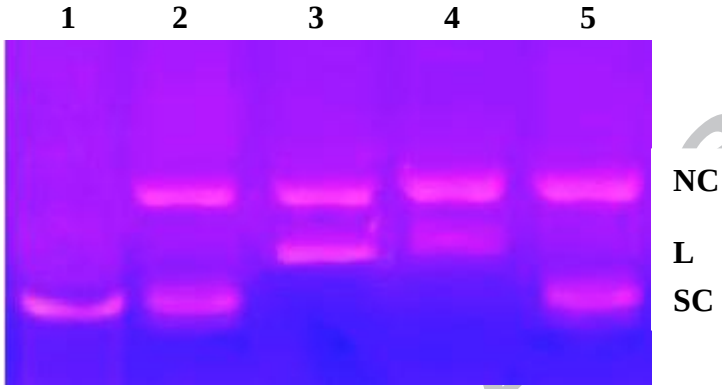

Fig. 8b. Gel electrophoresis pattern showing cleavage of pBR322 supercoiled DNA (10 μM) by Zn(II) complexes of L^1-L^4 in presence of SOD (1U). Lane 1: DNA alone; lane 2: 60 μM $[ZnL^3Cl_2]$ + DNA + SOD (1U); lane 3: 60 μM $[ZnL^1Cl_2]$ + DNA + SOD (1U); lane 4: 60 μM $[ZnL^2Cl_2]$ + DNA + SOD (1U); lane 5: 60 μM $[ZnL^4Cl_2]$ + DNA + SOD (1U).

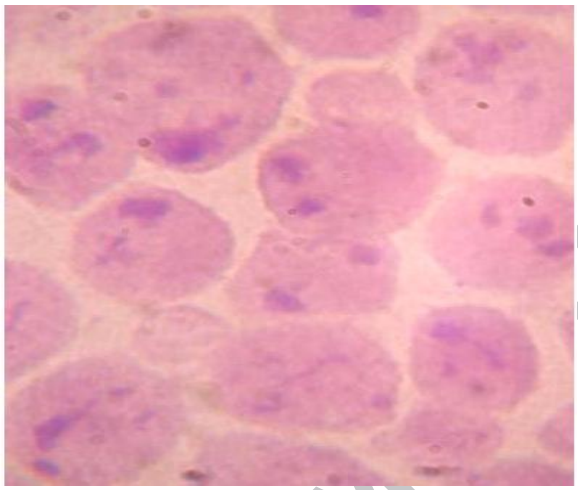

Fig.9a. Smear showing matured EAC control cells with definite cell wall and structure without degeneration.

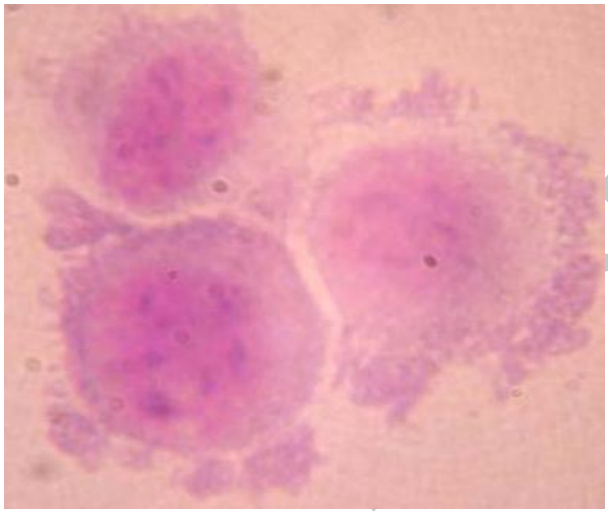

Fig.9b. EAC tumor cells showing degenerative changes in the form of membrane blebbing, cell wall fragmentation and low staining intensity.

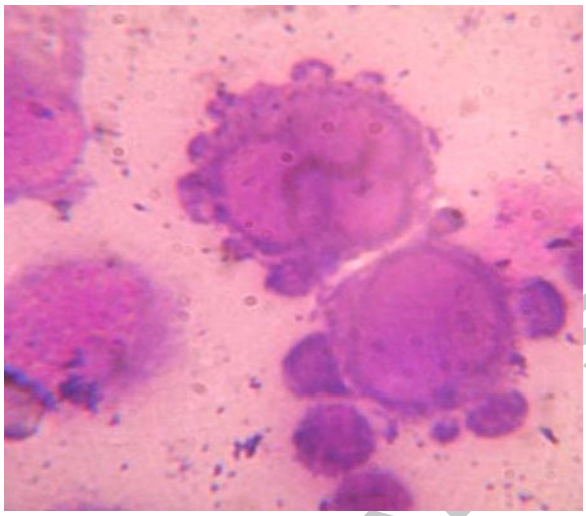

Fig.9c. Cu(II) complex of L^1 treated EAC Cells showing degenerative changes like membrane blebbing, vacuolated cytoplasm and low staining intensity with complete destruction of cells.

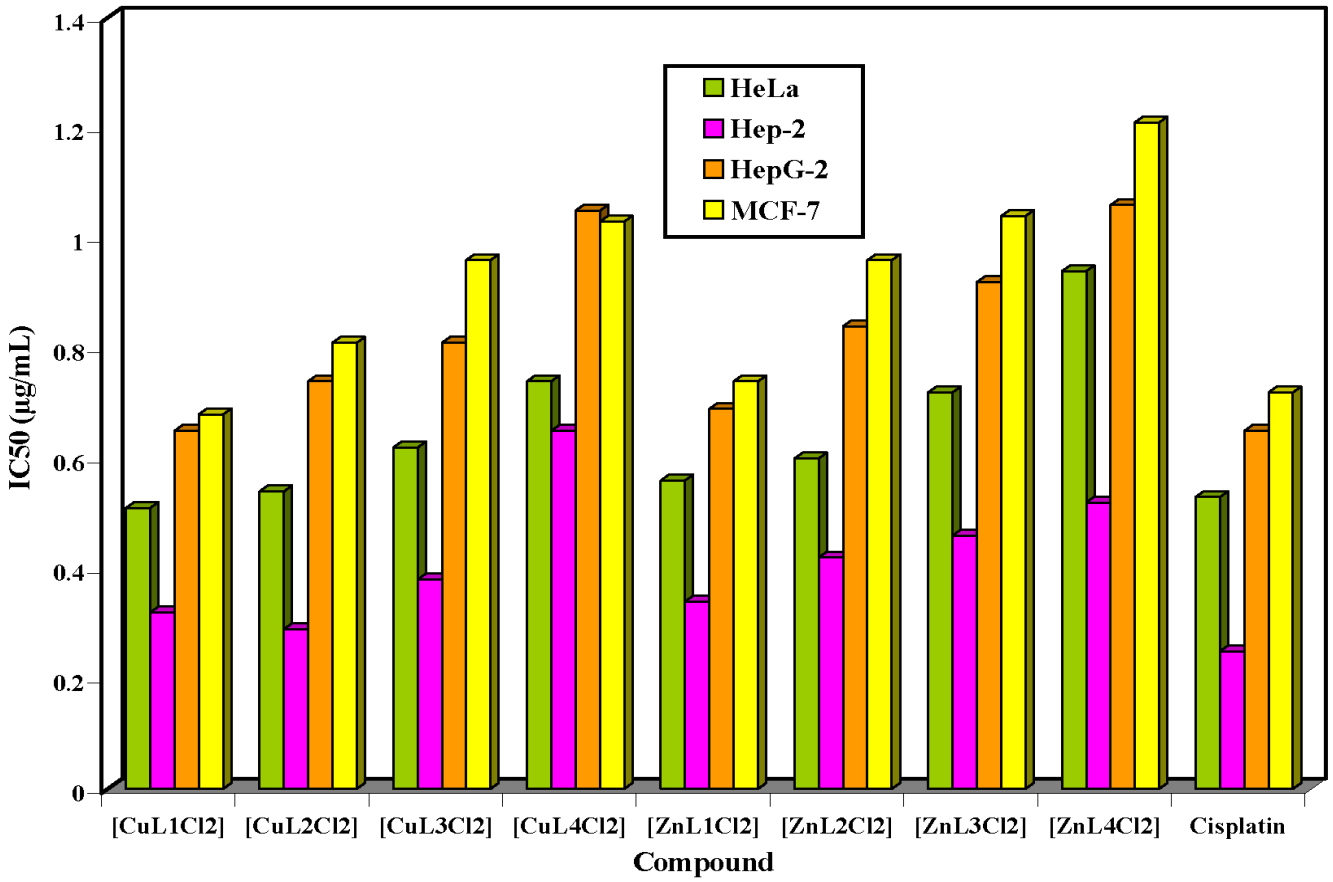

Fig. 10. IC_{50} (µg/mL) values of complexes and cisplatin against various cancer cell lines.

Table captions

Table 1 The spin Hamiltonian parameters of the Cu(II) complexes in DMSO solution at 77 K

Table 2 Electronic absorption spectral properties of ligands and their complexes

Table 3 Redox potential profiles for interaction of DNA with Cu(II) and Zn(II) complexes

Table 4 Minimum inhibitory concentration of the synthesized compounds against the growth of bacteria (μg/mL).

Table 5 Minimum inhibitory concentration of the synthesized compounds against growth of fungi (μg/mL).

Table 6 Antioxidant activity of the ligands and their complexes, Vitamin C and BHT against various radicals.

Table 7 SOD activity profile of synthesized metal complexes by NBT assay

Table 8 Effect of the complexes on hematological parameters of EAC tumor bearing mice.

Table 9 Effect of ligands and their complexes treatment on the survival of tumor-bearing mice

Table 10 *In vitro* cytotoxic activity of Cu(II) and Zn(II) complexes in EAC cell lines.

Table 11 IC_{50} (mg/mL) values of complexes and cisplatin against various cancer cell lines.

Table 1 The spin Hamiltonian parameters of the Cu(II) complexes in DMSO solution at 77 K

Complexes	**g-tensor**			**A × 10^{-4} (cm^{-1})**			$g_{\|}/A_{\|}$	**G**
	$g_{\|}$	$g_{\perp}$	g_{iso}	$A_{\|}$	$A_{\perp}$	A_{iso}		
$[CuL^1Cl_2]$	2.13	2.03	2.15	138	58	66	154	4.6
$[CuL^2Cl_2]$	2.21	2.04	2.11	135	54	72	162	4.8
$[CuL^3Cl_2]$	2.26	2.05	2.16	131	66	81	174	5.2
$[CuL^4Cl_2]$	2.22	2.04	2.14	132	39	69	168	5.0

Table 2 Electronic absorption spectral properties of ligands and their complexes

Complexes	λ_{max} (nm)		Δλ (nm)	%H	K_b (M^{-1})
	Free	Bound			
L^1	312.2	312.8	0.6	8	1.2×10^4
L^2	320.0	320.5	0.5	7	0.6×10^3
L^3	322.6	322.9	0.3	7	0.5×10^3
L^4	321.4	321.7	0.3	6	0.2×10^3
$[CuL^1Cl_2]$	364.5	366.0	1.5	10	1.5×10^5
$[CuL^2Cl_2]$	340.0	341.0	1.0	6	0.8×10^4
$[CuL^3Cl_2]$	355.5	356.8	1.3	8	0.6×10^4
$[CuL^4Cl_2]$	352.6	353.8	1.2	9	0.5×10^4
$[ZnL^1Cl_2]$	369.5	371.5	2.0	9	1.0×10^5
$[ZnL^2Cl_2]$	341.5	342.5	1.0	7	0.2×10^4
$[ZnL^3Cl_2]$	356.4	357.2	0.8	8	0.7×10^4
$[ZnL^4Cl_2]$	363.7	364.6	0.9	6	0.6×10^4

[a]$H\% = [A_{free} - A_{bound}) / A_{free}] \times 100\%$

[b]K_b = Intrinsic DNA binding constant determined from the UV - Vis absorption spectral titration

Table 3 Redox potential profiles for interaction of DNA with Cu(II) and Zn(II) complexes

Complexes	ΔEp (V)		$E_{1/2}$ (V)		I_{pa}/I_{pc}
	Free	Bound	Free	Bound	
$[CuL^1Cl_2]$	-0.230	-0.107	-0.121	-0.003	0.678
$[CuL^2Cl_2]$	0.695	0.678	0.299	0.266	1.226
$[CuL^3Cl_2]$	-0.111	-0.105	-0.172	-0.179	0.690
$[CuL^4Cl_2]$	0.352	0.428	0.176	0.366	0.927
$[ZnL^1Cl_2]$	-0.113	0.256	-0.043	-0.128	0.405
$[ZnL^2Cl_2]$	0.117	0.197	-0.850	-0.941	1.340
$[ZnL^3Cl_2]$	0.935	0.928	-0.065	-0.096	0.761
$[ZnL^4Cl_2]$	0.172	0.169	-0.045	-0.049	0.783

Data from cyclic voltammetric measurements: [a]$E_{1/2}$ is calculated as the average of anodic (E_{Pa}) and cathodic (Ep_c) peak potentials; $E_{1/2}{}^a = Ep_a + Epc / 2$; [b]$\Delta Ep = Ep_a - Epc$

Table 4 Minimum inhibitory concentration of the synthesized compounds against growth of bacteria (μg/mL).

Compound	Minimum inhibitory concentration (MIC) (× 10^4 μM)				
	Staphylococcus aureus	*Bacillus subtilis*	*Escherichia coli*	*Klebsiella pneumoniae*	*Salmonella typhi*
L^1	16.7	16.1	15.3	16.7	16.3
L^2	17.0	18.2	16.3	16.4	16.8
L^3	19.3	10.9	18.7	18.3	17.1
L^4	18.5	19.6	17.0	17.6	17.9
$[CuL^1Cl_2]$	10.2	10.7	8.9	8.4	9.6
$[CuL^2Cl_2]$	10.9	11.5	9.6	9.2	10.3
$[CuL^3Cl_2]$	11.4	12.1	10.5	10.1	11.0
$[CuL^4Cl_2]$	11.3	11.8	10.4	10.3	11.2
$[ZnL^1Cl_2]$	12.8	13.1	12.4	12.7	13.6
$[ZnL^2Cl_2]$	13.6	13.4	13.9	13.5	14.1
$[ZnL^3Cl_2]$	13.9	13.2	13.1	12.9	14.3
$[ZnL^4Cl_2]$	14.2	13.6	13.5	13.4	14.8
[a]Kanamycin	1.6	2.8	1.4	2.3	2.6

[a] Kanamycin is used as the standard

Table 5 Minimum inhibitory concentration of the synthesized compounds against the growth of fungi (μg/mL).

Compound	Minimum inhibitory concentration (MIC) (× 10^4 μM)				
	Aspergillus niger	*Fusarium solani*	*Curvularia lunata*	*Rhizoctonia bataicola*	*Candida albicans*
L^1	16.2	17.4	15.5	14.9	16.4
L^2	18.9	18.5	17.6	15.8	17.6
L^3	20.3	21.6	19.5	17.5	18.4
L^4	19.2	19.0	18.1	16.9	17.9
$[CuL^1Cl_2]$	12.5	14.2	12.9	13.8	14.5
$[CuL^2Cl_2]$	14.0	15.5	13.8	14.9	15.2
$[CuL^3Cl_2]$	15.2	17.4	15.1	16.8	15.8
$[CuL^4Cl_2]$	14.5	16.8	14.0	15.7	14.9
$[ZnL^1Cl_2]$	15.7	17.5	13.8	14.5	15.4
$[ZnL^2Cl_2]$	16.4	16.4	14.2	15.4	14.8
$[ZnL^3Cl_2]$	17.3	18.9	16.6	17.8	16.7
$[ZnL^4Cl_2]$	16.1	17.5	15.4	16.3	16.5
[a]Fluconazole	1.4	1.7	1.2	1.5	1.8

[a]Fluconazole is used as the standard

Table 6 Antioxidant activity of the ligands and their complexes, Vitamin C and BHT against various radicals.

Compounds	IC_{50}(μM)	
	DPPH·	**H_2O_2**
$[L^1]$	99.6 ± 1.2	102.3 ± 1.5
$[L^2]$	102.7 ± 1.6	104.2±0.9
$[L^3]$	104.3±1.9	109.8±1.2
$[L^4]$	107.4±0.8	111.5±1.5
$[CuL^1Cl_2]$	69.6 ± 0.2	65.5 ± 2.9
$[CuL^2Cl_2]$	71.4±0.5	68.4±1.6
$[CuL^3Cl_2]$	74.4 ± 1.3	70.9 ± 0.4
$[CuL^4Cl_2]$	77.5 ± 1.1	76.7 ± 1.6
$[ZnL^1Cl_2]$	72.3 ± 1.4	67.2 ± 0.7
$[ZnL^2Cl_2]$	75.6±0.7	73.4±1.3
$[ZnL^3Cl_2]$	81.2 ± 1.7	76.8 ± 0.4
$[ZnL^4Cl_2]$	81.3±1.4	83.5±0.5
Vitamin C	146.8 ± 3.6	215.3 ± 2.4
BHT	87.4 ± 2.2	143.6 ± 3.8

Table 7 SOD activity profile of synthesized Cu(II) and Zn(II) complexes by NBT assay

Complexes	[a]Concentration (μM)
$[CuL^1Cl_2]$	2.96 ± 0.04
$[CuL^2Cl_2]$	4.34 ± 0.06
$[CuL^3Cl_2]$	5.68 ± 0.04
$[CuL^4Cl_2]$	7.03 ± 0.03
$[ZnL^1Cl_2]$	3.26 ± 0.04
$[ZnL^2Cl_2]$	4.53 ± 0.06
$[ZnL^3Cl_2]$	6.74 ± 0.04
$[ZnL^4Cl_2]$	7.83 ± 0.03

[a]Equivalent to 1 U SOD (0.04 mM).

Table 8 Effect of Cu(II) and Zn(II) complexes on hematological parameters of EAC tumor bearing mice

Design of treatment	Hb (gm %)	RBC 10^6 Cells/CU.MM	WBC 10^3 Cells/CU.MM	Total protein mg%	PCV (%)	Differential count (%)		
						Lymphocytes	Neutrophils	Monocytes
Normal	12.92 ± 0.15	4.9 ± 0.12	6.78 ± 0.14	5.73 ± 0.26	16.86 ± 0.55	66.4 ± 1.36	32.6 ± 1.6	1 ± 0.45
Tumor control	5.78 ± 0.4[a]	2.46 ± 0.14[a]	18.74 ± 0.47[a]	12.23 ± 0.34[a]	25.98 ± 0.56[a]	26.2 ± 1.16[a]	72.8 ± 1.07[a]	1 ± 0.45
L^1	9.94 ± 0.3[b,d]	3.06±0.72[d]	9.05±0.07[a,d]	6.25±0.21[b,d]	21.04±1.02[d]	49.05±0.2[d]	45.63±0.08[d]	0.3±0.25
$[CuL^1Cl_2]$	12.09 ± 0.21[d]	4.15 ± 0.19[d]	15.54 ± 0.3[a,d]	7.14 ± 0.17[b,d]	17.06± 0.26[d]	64.2 ± 0.86[d]	35.2 ± 1.24[d]	0.6 ± 0.4
$[CuL^2Cl_2]$	11.38 ± 0.13[d]	3.44 ± 0.15[a,e]	14.96 ± 0.54[a,d]	7.62 ± 0.27[a,d]	16.98 ± 0.51[d]	68 ± 1.0[d]	31.6 ± 1.03[d]	0.4 ± 0.24
$[CuL^3Cl_2]$	11.04 ± 0.16[a,d]	3.94 ± 0.13[b,d]	12.16 ± 0.63[a,d]	8.56 ± 0.17[a,d]	17.1 ± 0.45[d]	63.2 ± 1.28[d]	36.2 ± 1.46[d]	0.6 ± 0.4
$[CuL^4Cl_2]$	13 ± 0.14[d]	4.04 ± 0.15[d]	11.4 ± 0.42[a,d]	7.96 ± 0.41[a,d]	19.98 ± 0.54[b,d]	61.4 ± 1.21[d]	38 ± 1.23[d]	0.6 ± 0.24
$[ZnL^1Cl_2]$	12.01 ± 0.29[d]	4.09 ± 0.21[d]	11.86 ± 0.32[a,d]	7.07 ± 0.24[b,d]	18.36 ± 0.43[d]	67.2 ± 1.93[d]	32.4 ± 2.11[d]	0.4 ± 0.4
$[ZnL^2Cl_2]$	11.1 ± 0.43[a,d]	4.2 ± 0.12[d]	12.54 ± 0.36[a,d]	8.14 ± 0.14[a,d]	17.2 ± 0.45[d]	65.6 ± 1.72[d]	33.8 ± 1.83[d]	0.6 ± 0.4
$[ZnL^3Cl_2]$	11.72 ± 0.27[d]	4.04 ± 0.21[c,d]	11.78 ± 0.32[a,d]	6.76 ± 0.23[d]	18.44 ± 0.71[d]	64.8 ± 1.28[d]	34.6 ± 1.63[d]	0.6 ± 0.4
$[ZnL^4Cl_2]$	12.23 ± 0.23[d]	3.92 ± 0.11[b,d]	11.04 ± 0.72[a,d]	7.06 ± 0.24[c,d]	18.04 ± 0.47[d]	64.6 ± 1.36[d]	35 ± 1.14[d]	0.4 ± 0.24

[a]P<0.001:; [b]P<0.01; [c]P<0.05 *versus* Normal

[d]P<0.001; [e]P<0.01 *versus* Tumor control. Data were analyzed by using one way ANOVA followed by Tukey-Kramer multiple comparison test.

Table 9 Effect of ligands and their complexes treatment on the survival of tumor-bearing mice

Treatment	MST	Increase in life span
Tumor control	14.56 ± 0.56	—
5- FU	34.83 ± 0.87*	140.21
L^1	23.49±0.43	64.34
L^2	21.67±0.72	61.48
L^3	20.94±1.03	58.23
L^4	18.76±0.78	55.87
$[CuL^1Cl_2]$	29.13 ± 0.60*	112.64
$[CuL^2Cl_2]$	28.25 ± 0.58*	111.69
$[CuL^3Cl_2]$	27.93 ± 0.75*	109.32
$[CuL^4Cl_2]$	27.85 ± 0.58*	108.91
$[ZnL^1Cl_2]$	29.27 ± 0.25*	112.86
$[ZnL^2Cl_2]$	28.97 ± 0.30*	101.17
$[ZnL^3Cl_2]$	27.64 ± 0.92*	105.72
$[ZnL^4Cl_2]$	27.36 ± 0.90*	102.07

N = 6; d of drug treatment = 9, *p < 0.01 *versus* tumor control.
Data were analyzed by one-way ANOVA followed by Dunnett's test.

Table 10 *In vitro* cytotoxic activity of Cu(II) and Zn(II) complexes in EAC cell line

Treatment compounds	**IC_{50} (μg/mL)**
$[CuL^1Cl_2]$	113.87
$[CuL^2Cl_2]$	112.95
$[CuL^3Cl_2]$	113.38
$[CuL^4Cl_2]$	110.18
$[ZnL^1Cl_2]$	112.89
$[ZnL^2Cl_2]$	108.35
$[ZnL^3Cl_2]$	105.40
$[ZnL^4Cl_2]$	106.56

Average of 3 determinations, 3 replicates
IC_{50}, Drug concentration inhibiting 50% cellular growth following 3 h of drug exposure.

Table 11 IC_{50} (mg/mL) values of complexes and cis-platin against various cancer cell lines.

Compounds	IC_{50} (µg/mL)			
	HeLa	Hep-2	HepG-2	MCF-7
$[CuL^1Cl_2]$	0.51	0.32	0.65	0.68
$[CuL^2Cl_2]$	0.54	0.29	0.74	0.81
$[CuL^3Cl_2]$	0.62	0.38	0.81	0.96
$[CuL^4Cl_2]$	0.74	0.65	1.05	1.03
$[ZnL^1Cl_2]$	0.56	0.34	0.69	0.74
$[ZnL^2Cl_2]$	0.60	0.42	0.84	0.96
$[ZnL^3Cl_2]$	0.72	0.46	0.92	1.04
$[ZnL^4Cl_2]$	0.94	0.52	1.06	1.21
cis-platin	0.53	0.25	0.65	0.72

Average of 3 determinations, 3 replicates
IC_{50}, Drug concentration inhibiting 50% cellular growth following 72 h of drug exposure.

Research Highlights

- A versatile synthesis of flexible conjugative chelating ligands is described.
- The chelator's role in determining the DNA cleavage behavior of copper complexes is explored.
- The synergic effect is observed between metal(II) centers.
- The Cu(II) complexes exhibit growth inhibitory activities better than cisplatin.
- Tumor cell cytotoxicity of ligands and complexes shows promising results.

Lasing the DNA fragments through β-diketimine framed Knoevenagel condensed Cu(II) and Zn(II) complexes – An *in vitro* and *in vivo* approach

Natarajan Raman,* Narayanaperumal Pravin

Research Department of Chemistry, VHNSN College, Virudhunagar-626 001, Tamil Nadu, India,

E-mail: ramchem1964@gmail.com Tel: +091-92451-65958
E-mail: pravinknp2012@gmail.com Tel: +091-9677846333

Novel metal based chelating complexes have been synthesized and screened for biological aspects. The *in vitro* antitumor properties of all the complexes are evaluated against few human cancer cell lines. *In vivo* antitumor activity exhibits copper complexes have potent antitumor activity against EAC tumor model.